CryoSat-2 swath interferometric altimetry for mapping ice elevation and elevation change

Elsevier Editorial System(tm) for Advances in Space Research

Manuscript Draft

Manuscript Number: ASR-D-17-00083R2

Title: CryoSat-2 swath interferometric altimetry for mapping ice elevation and elevation change

Article Type: SI: The CryoSat Mission

Keywords: Radar altimetry; CryoSat-2; IceSat; ERS; ENVISAT; Antarctica; Greenland; Iceland; Svalbard; Sub-glacial lakes; drainage; thinning; thickening; swath processing; interferometry; Cryosphere; Ice Sheet; ice shelves; Ice Caps; glaciers; DEM; surface elevation change; climate change; sea level change; surges; surface mass balance; time-series.

Corresponding Author: Dr. Noel Gourmelen,

Corresponding Author's Institution: University of Edinburgh

First Author: Noel Gourmelen

Order of Authors: Noel Gourmelen; MariaJose Escorihuela; Andrew Shepherd; Luca Foresta; Alan Muir; Albert Garcia-Mondejar; Monica Roca; Steven G. Baker; Mark R. Drinkwater

Abstract: For more than 25 years, satellite radar altimetry has provided continuous information on the state of the cryosphere and on its contribution to global sea-level rise. The technique typically delivers maps of ice-sheet elevation and elevation change with 3 to 10 km spatial resolution and seasonal to monthly temporal resolution. Here we show how the interferometric mode of CryoSat-2 can be used to map broad (5 km-wide) swaths of surface elevation with fine (500 m) spatial resolution from each satellite pass, providing a step-change in the capability of satellite altimetry for glaciology. These swaths of elevation data contain up to two orders of magnitude more surface elevation measurements than standard altimeter products, which provide single elevation measurements based on the range to the Point-Of-Closest-Approach (POCA) in the vicinity of the sub-satellite ground track. The swath elevations allow a more dense, statistically robust time series of elevation change to be formed with temporal resolution of a factor 5 higher than for POCA. The mean differences between airborne altimeter and CryoSat-2 derived ice sheet elevations and elevation rates range from -0.931.17 m and 0.291.25 m a-1, respectively, at the POCA, to -1.501.73 m and 0.041.04 m a-1, respectively, across the entire swath. We demonstrate the potential of these data by creating and evaluating elevation models of: (i) the Austfonna Ice Cap (Svalbard), (ii) western Greenland, and (iii) Law Dome (East Antarctica); and maps of ice elevation change of: (iv) the Amundsen Sea sector (West Antarctica), (v) Icelandic ice caps, and (vi) above an active subglacial lake system at Thwaites Glacier (Antarctica), each at 500 m spatial posting - around 10 times finer than possible using traditional approaches based on standard altimetry products.

CryoSat-2 swath interferometric altimetry for mapping ice elevation and elevation change

N. Gourmelen[1,2], M.J. Escorihuela[3], A. Shepherd[4], L. Foresta[1], A. Muir[5], A. Garcia-Mondejar[3], M. Roca[3], S.G. Baker[5], M.R. Drinkwater[6]

1. School of GeoSciences, University of Edinburgh, Drummond Street, Edinburgh EH8 9XP, UK

2. IPGS UMR 7516, Université de Strasbourg, CNRS, Strasbourg 67000, France

3. isardSAT, Guildford GU2 7YG, UK

4. Centre for Polar Observation and Modelling, School of Earth and Environment, University of Leeds, Leeds LS2 9JT, UK

5. Centre for Polar Observation and Modelling, Department of Earth Sciences, University College London, Gower Street, London WC1E 6BT, UK

6. European Space Agency, ESA-ESTEC, Kelperlaan 1, 2201 AZ Noordwijk, Netherlands

1. Abstract

For more than 25 years, satellite radar altimetry has provided continuous information on the state of the cryosphere and on its contribution to global sea-level rise. The technique typically delivers maps of ice-sheet elevation and elevation change with 3 to 10 km spatial resolution and seasonal to monthly temporal resolution. Here we show how the interferometric mode of CryoSat-2 can be used to map broad (5 km-wide) swaths of surface elevation with fine (500 m) spatial resolution from each satellite pass, providing a step-change in the capability of satellite altimetry for glaciology. These swaths of elevation data contain up to two orders of magnitude more surface elevation measurements than standard altimeter products, which provide single elevation measurements based on the range to the Point-Of-Closest-Approach (POCA) in the vicinity of the sub-satellite ground track. The swath elevations allow a more dense, statistically robust time series of elevation change to be formed with temporal resolution of a factor 5 higher than for POCA. The mean differences between airborne altimeter and CryoSat-2 derived ice sheet elevations and elevation rates range from -0.93±1.17 m and 0.29±1.25 m a^{-1}, respectively, at the POCA, to -1.50±1.73 m and 0.04±1.04 m a^{-1}, respectively, across the entire swath. We demonstrate the potential of these data by creating and evaluating elevation models of: (i) the Austfonna Ice Cap (Svalbard), (ii) western Greenland, and (iii) Law Dome (East Antarctica); and maps of ice elevation change of: (iv) the Amundsen Sea sector (West Antarctica), (v) Icelandic ice caps, and (vi) above an active subglacial lake system at Thwaites Glacier (Antarctica), each at 500 m spatial posting – around 10 times finer than possible using traditional approaches based on standard altimetry products.

2. Introduction

Earth's land ice, including the Greenland and Antarctic Ice Sheets (GrIS and AIS respectively), ice caps and mountain glaciers, is losing mass, and is estimated to have contributed 31 mm towards global sea-level rise since 1992 (Shepherd et al. 2012, Gardner et al. 2013, IPCC 2013). During this period, satellite altimetry has revolutionised our ability to continuously monitor changes affecting the cryosphere, providing novel and critical observations to detect, monitor, quantify and understand land ice mass balance, sub-glacial water routing, ice-ocean interactions, and current and potential sea-level contribution (e.g. Zwally et al. 1989, Wingham et al. 1998, Shepherd et al. 2001, Shepherd et al. 2003, Zwally et al. 2005, Wingham et al. 2006a, Fricker et al. 2007, Pritchard et al. 2009, Wilson et al. 2010, Kaab et al. 2012, Bamber et al. 2013, McMillan et al. 2014b, Gourmelen et al. 2017). Nevertheless, pulse-limited altimetry was designed for ocean applications, and the relatively coarse ground resolution that can be achieved with the technique has been a limiting factor for glaciology - in particular when assessing changes in coastal sectors of the ice sheets and in mountain glaciers and ice caps (Dehecq et al. 2013). The ground resolution of early altimeter missions was limited by several factors, including the pulse- (1.6km) and beam- (10-20 km) limited footprint size of radar altimeters, the relatively large separation of ground tracks (e.g. 20 km across track speration for IceSat at 70^{o} of latitude) (Gourmelen et al. 2017), and the inability to pinpoint the location of echoes on sloping terrain.

The CryoSat-2 mission, launched by ESA in 2010, achieves improved ground resolution in three ways; the satellite benefits from a tight ground track network (7.5 km at the equator, 1.6 km at 70^{o} of latitude), the radar employs Synthetic Aperture Radar (SAR) processing in the along-track direction to achieve a much reduced pulse-Doppler-limited along-track footprint and resolution of 305m and 400 m, respectively (over a flat surface); and a second receiver antenna allows the across-track location of the

ground echo to be precisely determined via radar interferometry (Drinkwater et al. 2005, Wingham et al. 2006). The so-called SAR Interferometry (SARIn) mode is activated above all land ice with a significant surface slope (e.g. ice sheet margins, ice caps, mountain glaciers) and provides an exact solution to the echo location uncertainty over sloping terrains (Brenner et al. 1983). Together, these advances allow CryoSat-2 to survey small and rugged areas of ice covered terrain, providing 5 and 6 times more data than ICESat and Envisat, respectively (McMillan et al. 2014b). A shared characteristic of standard radar altimetry methods is, however, that they all rely on the determination of the Point-Of-Closest-Approach (POCA), sampling a single elevation beneath the satellite. Here, we present a method for determining ice elevation across extended swaths of terrain utilising the information contained within CryoSat-2 altimeter SARIn echoes.

The Interferometric mode of CryoSat-2 provides the ability to resolve substantially more than just the elevation at the POCA. If the ground terrain slope is only a few degrees, the CryoSat-2 altimeter operates in a manner such that the interferometric phase of the altimeter echoes may be unwrapped to produce a wide swath of elevation measurements across the satellite ground track beyond the POCA (Wingham et al. 2006, Hawley et al. 2009), referred to in the remainder of this manuscript as L2swath or simply swath (Figure 2).

An early proof of concept was performed on data acquired by the ASIRAS airborne prototype of the CryoSat-2 instrument over the Austfonna ice cap, Svalbard, in the spring of 2004 (Hawley et al. 2009). When evaluated against Airborne Laser Scanner (ALS) data, swath elevations show a root mean square (RMS) departure of 1.67m in contrast to 1.33m when only extracting the POCA. However, swath processing provided up to 2 orders of magnitude more elevation measurements than at the POCA alone. A study performed using CryoSat-2 data over a western section of the Devon Ice Cap

identified similar relative accuracy between swath and POCA (Gray et al. 2013). Recent applications have shown the potential of the technique to image thinning rates at ice sheet margin (Christie et al. 2016), surface depression related to supra-glacial lakes (Ignéczi et al. 2016), surface elevation change related to sub-glacial lakes drainage (Smith et al. 2016), ice caps mass balance (Foresta et al. 2016), and basal melting under ice-shelf (Gourmelen et al. 2017) with much greater surface details.

Here, we describe a method to derive swath elevation from the SARIn mode of CryoSat-2, and illustrate the benefit of the approach to derive surface elevation and time-dependant surface elevation change. We present experimental elevation and elevation change products derived from swath processing over several sites in the GrIS, AIS and over ice caps in Iceland and Svalbard. We present validation results and compare the swath measurements and derived products with existing datasets generated from conventional CryoSat-2 POCA technique, as well as datasets generated from past and present optical and radar airborne and spaceborne missions.

3. Data and methods

3.1. Swath interferometric altimetry

The swath algorithm consists of (i) identifying suitable waveform echoes within the L1b SARIn mode product based on high phase coherence, amplitude and surface slopes, the threshold to use will depend on the local conditions (Gray et al. 2013, Foresta et al. 2016, Gray et al. 2016); (ii) determining the correct phase ambiguity (unwrapping) (as wrapping of the phase occurs for an arrival angle greater than $\sim 0.54^{o}$) by a combination of spatial unwrapping and quality control using a reference digital elevation model (Gray et al. 2015, Foresta et al. 2016) and (iii) mapping the range, across-track look

angle, platform attitude and orbit parameters of each echo into a swath comprised of multiple elevation points above a reference ellipsoid (Figure 3) (Wingham et al. 2006, Hawley et al. 2009, Gray et al. 2013, Foresta et al. 2016).

3.1.1. Input data

Swath processing takes as input multi-looked echo (L1b product, baseline C) from the Synthetic Aperture Radar Interferometric (SARIn) mode of CryoSat-2, containing the power, interferometer phase and coherence waveforms. All necessary input data are contained in the L1b product delivered by ESA (ftp://science-pds.cryosat.esa.int) with the exception of an external reference digital elevation model (DEM_{ref}).

3.1.2. Smoothing

To reduce instrument noise, the phase and amplitude are filtered by recreating the interferogram, filtering its real and imaginary components with a low pass filter and retrieving the phase from the smoothed interferogram (Gray et al. 2013). We filter each waveform independently with a filter size equal to 3 bins to limit the loss of spatial resolution.

3.1.3. Local phase unwrapping

Phase difference can only be known within a [-π π] interval and so a phase ambiguity will be present when the angle of arrival exceeds about half a degree, a situation that can occur when e.g. the ground-surface slope exceeds about half a degree. Correction of phase ambiguities requires a phase unwrapping procedure which is applied to each waveform separately by adding or subtracting 2π when the absolute phase change between 2 consecutive bins exceeds π. In order to minimize phase unwrapping errors, phase values for which the coherence is below a threshold of 0.8 is masked.

3.1.4. Generation of Latitude, longitude and elevation

The look angle θ is such that

$$\theta = \arcsin\left(-\frac{\lambda}{2\pi}\frac{\delta\varphi}{B}\right) - \beta \qquad (1)$$

with λ the wavelength, $\delta\varphi$ the phase difference, B the interferometer baseline and β the roll angle. The range R at each waveform sample n as:

$$R(n) = \frac{c}{2}\cdot\left(T + \frac{1}{2\cdot F_r}\left(n - \frac{N}{2}\right)\right) \quad (2)$$

where N is the total number of waveform samples, n is the sample number in the [0, N-1] interval, T is the window delay, in seconds, at bin $\frac{N}{2}$, F_r is the instrument sampling frequency, and c is the speed of light.

3.1.5. Global phase unwrapping

We introduce an additional step to account for phase ambiguities; the independent DEM_{ref} is used to guide the phase unwrapping steps where phase ambiguity cannot be resolved from simple unwrapping (e.g. when the entire waveform is affected by a phase ambiguity). This approach potentially improves the measure of elevation for echoes whose across-track angle is above $\sim 0.54^{o}$ for all or part of the beam limited footprint, a condition found frequently for ice caps and locally along ice sheet margins.

In the presence of slopes exceeding $\sim 0.54^{o}$, the conventional unwrapping procedure described above will not be able to resolve the phase ambiguity as the first arrival measurement will be affected by a phase shift; in this situation we will need to apply a 'global' phase correction, i.e. adding or subtracting a suitable multiple of 2π to the phase values of a waveform. Without accounting for this correction, elevation estimates can be off by tens of meters and their location off by a few kilometers.

We implemented a procedure involving a reference DEM. For each waveform, latitude, longitude and elevation are computed for a number of 2π multiples (positive and negative). The correct 2π ambiguity is then chosen using two metrics. Firstly, we find the phase ambiguity that minimizes the elevation difference between CryoSat-2 swath and the DEM_{ref}:

$$\sum_{i=1}^{N} \left| h_i - DEM_{ref_i} \right| \quad (3)$$

with h_i and DEM_{ref_i} respectively the swath elevation and DEM_{ref} at the waveform sample number i. The second metric is the dispersion of the elevation difference defined as the Median Absolute Deviation:

$$MAD_{hd} = median|hd - median(hd)| \quad (4)$$

where hd is a vector of the difference between the swath elevations at each waveform samples and the corresponding reference elevation. This second metric stems from the fact that an erroneous phase ambiguity will impact on the slope of the surface topography, hence leading to a large value of MAD_{hd} (Figure 4). This second metric adds robustness to the determination of the phase ambiguity.

Given the magnitude of the impact of a phase ambiguity on the planimetric positioning, elevation and surface slope of the swath measurement (Figure 4), and although the reference DEM need to be relatively accurate or recent, a certain level of difference is acceptable. However, due to the complexity of surface terrain it is difficult to predict the level of accuracy needed. Distinct reference DEMs are used in this study for GrIS (Howat, Negrete & Smith 2014), AIS (Fretwell et al. 2013), Iceland (Landmælingar Íslands, www.lmi.is), and Svalbard (McMillan et al. 2014a).

We note that phase ambiguity is not only affecting swath but also POCA processing were a reference DEM is also needed to resolve phase ambiguity (Gray et al. 2015).

3.2. Digital elevation model and rates of surface elevation change

Because of the increased data density, L2swath altimetry provides a capability to determine changes in ice elevation at the maximum spatial resolution of the CryoSat-2 instrument, up to 0.4 km in the platform's along-track direction. To assess this capability, we computed ice sheet surface elevation changes within 500 m grid cells by fitting a plane to the raw L2swath elevation measurements within a grid cell using a model function of spatial and temporal elevation change of the form:

$$Z(x, y, t) = ax + by + c + dt \qquad (5)$$

where Z is the swath elevation, x and y are the easting and northing coordinates of each swath data point, respectively, and t is the time of data acquisition (Foresta et al. 2016). Surface elevation and elevation change are then determined from the model parameters a, b, c and d; a corresponding to the eastward linear elevation trend, b to the northward linear elevation trend, c a constant, and d the linear rate of temporal elevation change. In this model the spatial variation in elevation is determined as a bilinear function and the temporal variation of elevation as a linear term. The power field, P, is used to weight the individual elevation measurements during the inversion process; for each grid cell, the weight, w, is defined as:

$$w = \frac{P^2}{\max(P)^2} \qquad (6)$$

This weighting strongly penalises measurement with low power. This inversion approach is similar to solutions applied to CryoSat-2 POCA data (McMillan et al. 2014b), only with a simplification of the terrain slope terms made possible by the finer spatial distribution of the input data. The use of either linear or quadratic polynomial to model

the terrain slope within a grid cell does not affect markedly the values of elevation change compared to airborne data, with less than 1% difference under each scenario.

The advantage of this approach to determine a gridded CryoSat-2 swath digital elevation model (CSDEM), with respect to other approaches that average measurements acquired over a long time-period, is the ability of our model to account for the time-dependant aspect of the topography in regions of rapid and complex changes, and therefore to generate a DEM of high-temporal fidelity.

3.3. Validation

Swath elevation and derived gridded products are validated using surface elevation and elevation change from the NASA Operation IceBridge (OIB) Airborne Topographic Mapper (ATM) campaigns (Krabill 2016, Krabill 2015). OIB campaigns are a series of airborne missions to map Arctic and Antarctic ice sheets with laser altimetry between 2009 and 2016 (filling the gap between ICESat and ICESat-2). We have used the OIB ATM L2 Icessn Elevation, Slope, and Roughness product, Version 1. The ATM data are referenced to the ITRF-2005 reference frame and projected onto the WGS-84 ellipsoid. The footprint size of each individual elevation measurement is 1 m, which is set by the laser beam divergence (Krabill 2016). Absolute elevation accuracy from the ATM is usually about 10 cm or better (Krabill 2016) with geolocation accuracies of better than 1 m (Schenk, Csatho & Lee 1999). Specifically for the OIB campaigns, the parameters of the ATM system are estimated to be (i) 74 cm horizontal accuracy, (ii) 6.6 cm vertical accuracy, and (iii) 3 cm vertical precision (Martin et al. 2012).

Due to the rapid changes at the margins of the ice sheets, only elevation data acquired as close in time as possible has been considered for validation purposes. The validation activities have also avoided rapid melting and precipitation periods and have been

therefore concentrated for the northern hemisphere in the months of March, April and May and for the Southern Hemisphere in the months of October and November covered by OIB ATM acquisitions.

For each CryoSat-s measurement we select the nearest validation measurement that satisfies the spatial and temporal baseline thresholds of 50m and 10 days respectively. For the gridded CSDEM and rates of elevation change products, the spatial criterion is that the validation measurement is within half the grid spacing, or 250m, and the temporal criterion is 1 repeat cycle (369 days) from the time stamps of the CSDEM which are usually set at the first CryoSat-2 record, i.e. 07/2010. We then define a measurement bias as the median value of the difference between the L2swath and the validation elevation, and a measurement dispersion as the Median Absolute Deviation defined as:

$$\mathrm{MAD} = \mathrm{median}(|(\mathrm{Z}_n - \mathrm{Z}_n^{val}) - \mathrm{median}(\mathrm{Z}_n - \mathrm{Z}_n^{val})|) \qquad (7)$$

where Z_n are the swath elevations and Z_n^{val} are the corresponding validation records.

Our validation test sites are located at the margins of the two ice sheets and include the glaciers of Petermann and Jakobshavn glaciers (GrIS), and the Pine Island and Thwaites glaciers in the Amundsen Sea sector of AIS.

4. Results

4.1. Swath elevation

4.1.1. Data coverage and volume

A capacity to sample elevation at locations beyond the POCA means that L2swath provides a snapshot of terrain in both along-track and across-track directions, turning CryoSat-2 into an instantaneous two-dimensional mapping sensor. The across-track width of swaths can reach several kilometres, the exact extent depending on surface

slope (Figure 5). Considering a range of glaciological targets, L2swath processing typically retrieves between 10 and 100 distinct elevation measurements from a single altimeter echo, by contrast to a single elevation measurement in the standard L2 product. The improvement in data quantity for each of the validation sites is provided in Table 1.

4.1.2. Validation

We evaluated the accuracy of L2swath data over GrIS and AIS marginal regions with respect to 344 x 10^3 independent airborne altimeter elevation measurements acquired between 2011 and 2014 (Figure 8 & Table 1). The differences between the airborne and CryoSat-2 swath elevations is -1.50 ± 1.73 m; the -1.5 m bias reflects the greater penetration of Ku-band radar into the snow and firn compared to the ATM. For comparison, the differences between the airborne and POCA observations is -0.93 ± 1.17 m.

4.1.3. Baseline C versus baseline B

In 2015, CryoSat-2's Instrument Processing Facilities was updated to Baseline C, improving the product's quality and correcting several biases (Scagliola, Fornari 2015). One improvement included in Baseline C is the removal of the waveform cut initially introduced in Baseline B during the oversampling of the 20 Hz waveform, that led to a loss of information. Baseline C now provides a range window of 240 m, double in length to that of baseline B. This leads to an increase in the number of elevations that L2swath is able to deliver (Figure 6).

4.1.4. Roll bias

An inaccurate value of satellite's roll angle will impact on the positioning of the elevation measurements, with a greater impact with large off-nadir angle. A roll bias of

0.1062° was identified in CryoSat's baselineB dataset and corrected in CryoSat new latest release, baseline C (Scagliola, Fornari 2015). It has been suggested that a residual roll bias is present in CryoSat's baseline C (Gray et al. 2016). To explore this possibility, we calculate swath elevations using look angles calculated by introducing arbitrary roll angle biases β_b as follows:

$$\theta = \arcsin\left(-\frac{\lambda}{2\pi}\frac{\delta\varphi}{B}\right) - (\beta + \beta_b) \qquad (8)$$

We then use OIB elevation to explore the roll angle bias impact on the L2swath-OIB elevation differences (Figure 7). When a roll angle bias is present, ascending and descending orbit will be affected in opposite direction leading to a double-peak histogram of the L2swath-OIB elevation differences (Figure 7, lower-left). For a correct value of roll angle, the histogram will have the expected single peak (Figure 7, lower-left). We then solve for the roll bias that minimises the histogram dispersion and found a value of 0.007° m. If uncorrected, this directly translates in an offset of 87 m in geolocation in the across track direction, and in a vertical offset of 0.01 m at nadir and of 1.60 m at the edge of the footprint, of the elevation retrieval.

This value is likely to vary however as the roll bias depends on the temperature of the platform. There are two causes of temperature changes: short term variations (the platform is facing the sun with different incidents angles within an orbit) and long term variation (the orbit plane of the platform has different incidents angles within the 369 day cycle).

The noise of the roll is higher when the measurements are given by the Star Tracker that is not the coldest, but also there is a long-term variation due to the bending of the bench where the Star Tracker are placed.

The new CryoSat-2 baseline-C incorporates a Star Tracker processor in charge of computing the attitude measurements provided on the products with the stated roll bias and some smoothing algorithms. With that smoothing the noise of the roll measurement is compensated but the long-term variation cannot be addressed at it would require a long term analysis. The external calibration analysis using data over a Transponder indicates that the roll bias in Baseline C is 0.0069 ± 0.003° (A.Garcia-Mondejar et al., 2017).

A dataset of re-calibrated attitude information recently released by ESA (https://earth.esa.int/web/guest/missions/esa-eo-missions/cryosat/str-attref) is also tested (Figure 7) and show that it largely corrects for the roll angle bias observed in the current baseline C dataset. The updated attitude will be incorporated in an upcoming baseline D release by ESA.

This exercise also demonstrates that swath processing could be a complementary approach to transponders for calibrating the attitude of interferometric radar altimeters with vastly improved spatial and temporal coverage.

4.2. Gridded Digital elevation model and rates of surface elevation change

We generated and validated gridded DEMs and rates of surface elevation change at 500 m grid spacing for the Jakobshavn area (west GrIS) and for the Amundsen Sea sector of West Antarctica. In total we retrieve an elevation for 98.8% (Jakobshavn area) and 98.2% (Amundsen Sea sector) of the area over the grounded ice sheets. For comparison, studies at the scale of the entire AIS using CryoSat-2 POCA data found 96% coverage at 5 km by 5km, and from Envisat cross-over POCA found 32% coverage at 10 km by 10km (Shepherd et al. 2012, McMillan et al. 2014b). We also show case examples over the Law Dome (East Antarctica) as well as over ice caps in Iceland.

4.2.1. Digital elevation model

Validation of the L2swath DEM at 500 m grid spacing indicates a bias of -1.4 m and a dispersion of 1.8 m when swath elevation are compared to 39,139 collocated airborne measurements from OIB over the Jakobshavn area (Figure 8). A similar intercomparison over the Amundsen Sea sector indicates bias of -1.7 m and a dispersion of 2.0 m when compared to 29,362 airborne measurements over grounded ice (Table 1) and -1.5 m and a dispersion of 1.2 m over floating ice (Gourmelen et al. 2017). Improved spatial resolution offered by the greater density of swath measurements allows far greater definition of glacial terrain than has been possible to date. For example, at Law Dome in East Antarctica, a CSDEM produced at 500 m grid spacing (Figure 9) clearly identifies surface features on length scales of 500 to 4000 m which are common in airborne data sets, but are not resolved in continental-scale products (Fretwell et al. 2013). Over the east flank of law Dome, a system of surface gashes is well defined at 500 m resolution; the gashes' system is the surface expression of a large canyon system in the underlying bedrock (Figure 9).

4.2.2. Surface elevation change

4.2.2.1. Multi-annual change

In the Amundsen Sea Sector of West Antarctica, rates of elevation change determined from L2swath show a remarkable level of detail when compared to results that can be achieved using POCA elevation data alone (Figure 10 & Figure 11). Although CryoSat-2 POCA data are recorded within a much smaller ground footprint than conventional pulse-limited altimetry, they lead to only a modest (factor 2) improvement in spatial resolution of elevation changes due to the relatively long orbit repeat cycle which requires measurements to be collated in space. In contrast, L2swath data allow for a 10-

fold improvement in spatial resolution of elevation changes (Table 1). Measurements with such fine sampling allow the detailed pattern of thinning along tributaries of the Pine Island, Thwaites, Smith, Kohler and Pope Glaciers to be clearly identified, and ensure that signals of elevation change can be retrieved up to the ice sheet margin even over the floating ice shelves (Gourmelen et al. 2017). Over smaller features such as ice caps the benefit of L2swath is also apparent with a dramatic increase in surface coverage (Figure 11). When comparing L2swath-derived rates of elevation change with POCA-derived estimates and with estimates of elevation change determined from repeat airborne surveys over the same period (Krabill 2015), the L2swath data are in excellent agreement. For the Amundsen Sea Sector (Figure 10), we observe a mean difference between swath and OIB of 0.04 ± 0.92 m a^{-1}, this value is comparable to the estimated certainty (0.40 ± 0.95 m a^{-1}) of POCA-derived elevation changes in the same region (McMillan et al. 2014b). Over ice caps we also observe a very good agreement and no noticeable impact of surface slopes (Figure 12) (Foresta et al. 2016).

4.2.2.2. Seasonal or transient change

CryoSat's repeat cycle of 369 days limits the temporal resolution at which localised changes can be mapped. Generating swath of elevation instead of POCA leads to overlap between adjacent tracks, leading to an increase in the temporal resolution at which elevation change can be determined. The improvement in spatial resolution is greater for deformation that are spatially and temporally localised. With L2swath data, we observe a 35-fold increase in the probability of sampling an area of 500 m^2 in size at 1-90 day time step (length of CryoSat-2's orbital sub-cycle) (Figure 13).

For example, the L2swath observations clearly identify a cluster of dislocated sites in the interior of the Thwaites Glacier drainage basin (Figure 14) (Smith et al. 2016). In

this 860 km^2 region, four sites of between 100 and 360 km^2 have lowered by 6 to 13 m over a 1 year period, similar to patterns of surface lowering above subglacial lakes that have drained in other sectors of Antarctica (Fricker et al. 2007, Wingham et al. 2006b). Observations using POCA data only partially cover the area (Figure 14) leading to an incomplete mapping of the subsidence features and a 30% error in the total subsidence volume.

A second example of highly-localised and rapid changes in ice elevation mapped by forming and differencing sequential CryoSat-2 L2swath measurements is shown in Figure 15. In the summer of 2014, the north-west sector of the Vatnajökull ice cap in the region of the Bárðarbunga caldera, Iceland, experienced high seismic activity followed by a volcanic eruption off-ice north of the seismic swarm (Sigmundsson et al. 2015). The entire caldera deformation was imaged by 6 swaths of CryoSat-2 data acquired just before and after the event, revealing the extent of the subsidence that affected the region of the ice cap in the months following the seismic activity (Figure 15). The L2swath data reveal that a 25 km^2 region subsided by over 40 m in the 4 months that followed the onset of seismic activity, amounting to a 0.75 km^3 deflation which has been confirmed by Airborne LIDAR and GPS surveys (Reykjavik Institute of Earth Sciences). The width of the swath was sufficient to map the entire subsidence event, when POCA elevation data would only have provided a coarse picture.

Seasonal patterns of elevation change, e.g. related to the seasonal cycle of accumulation and ablation, have been retrieved from altimetry over large region, at the scale of an entire ice sheet (McMillan et al. 2016) or ice cap (Gray et al. 2015). Increase spatial resolution means that we can start focussing seasonal analysis from radar altimetry over smaller targets. An example over the Vatnajökull ice cap (Iceland) shows the seasonal pattern in elevation related to accumulation and ablation partitioned between

the accumulation (above 1200 m) and ablation area (below 1200m) (Figure 16) (Foresta et al. 2016).

5. Discussion

The separation of CryoSat-2's ground track ranges from 7.5 km at the equator to less than 1.6 km at latitudes higher than 70°. However, the actual separation of elevation measurements recorded by the altimeter can be significantly larger than this, because the POCA is dependent upon the surface slope and tends to follow topographic ridges. This effect occurs in marginal sectors of the polar ice sheets and ice caps and across mountain glaciers, where the terrain is typically steep. In such instances, features that are kilometre-scale or smaller may be under-sampled or missed altogether by standard altimeter measurements recorded at the POCA alone. L2swath data, however, overcome this problem because they map broad and continuous swaths of ice covered terrain, allowing surface elevation and surface elevation changes to be determined with 10 times finer spatial resolution than conventional altimetry (Figure 9).

In addition to providing a denser network of elevation measurements around the POCA, swath interferometry allows for the retrieval of elevation data where the conventional POCA altimetry approach fails. This situation occurs where the POCA falls on incoherent surfaces, leading to retracker failure, or in regions of complex ice topography where the POCA tends to concentrate along topographic highs leaving topographic lows uncharted (McMillan et al. 2013). In contrast, L2swath is able to image the ice terrain beyond the POCA and to measure elevation in surface depressions providing they are within the limits of the altimeter's sampling window (corresponding to 240 m elevation range for CryoSat-2 baseline C).

The step-change in the yield of valid elevation measurements means that L2swath provides an opportunity to extract continuous surface elevation at enhanced spatial resolution in comparison to previous altimetry-based products (Fretwell et al. 2013, DiMarzio et al. 2007a, Bamber, Gomez-Dans & Griggs 2009). Although digital elevation models (DEMs) are often distributed on fine (500 to 1000 m) spatial grids, actual observations are generally oversampled. The effective resolution of existing products is typically an order of magnitude lower (DiMarzio et al. 2007a, DiMarzio et al. 2007b, Griggs, Bamber 2009), and many grid points are not constrained by measurements at all due to the paucity of primary observations. In addition to improved coverage, the accuracy of DEM's derived from swath altimetry is also well within that of existing products. The example elevation models we have produced demonstrate that continuous DEM's exhibiting true sub-kilometre spatial resolution are feasible with swath interferometric altimetry. The technique is now approaching the capabilities of airborne surveys (Howat, Negrete & Smith 2014, Krabill 2016), and while the spatial resolution of the gridded products obtained here is not commensurate with that achieved by high-resolution sensors (Berthier et al. 2014, Howat et al. 2015, A. Dehecq et al. 2016), the technique benefits from frequent and regular, day-night, all-weather and global coverage as well as seamless aggregation. We also note that the non-gridded swath product can resolve elevation at meter-scale spatial resolution (Gray et al. 2016) in par with high-resolution imaging sensors. As a consequence of the increased spatial sampling, L2swath data allow ice elevations to be mapped with higher temporal frequency. Although the CryoSat-2 orbit repeat cycle is 369 days, which limits the observation of rapidly changing processes, the width of L2swath swaths provides greater overlap between adjacent ground tracks. At 70^{o} latitude this translate into a three, five, ten and 35-fold increase in temporal sampling respectively at 5, 3, 1 and 0.5

km posting when compared to POCA measurements alone (Figure 13). Improved sampling of ice elevation changes will improve our understanding of key glaciological processes. Although half of today's sea level change is due to ice mass losses (IPCC 2013), these losses are predominantly occurring in mountainous and coastal regions which present a challenge to conventional altimetry. However, because L2swath performs well over rugged ice covered terrain, more accurate estimates of glacier and ice sheet mass balance will become possible. The movement of water between lakes at the base of the Antarctic (Fricker et al. 2007, Wingham et al. 2006b) and Greenland (Joughin et al. 1996) ice sheets, has the capacity to affect ice flow (Smith et al. 2016, Stearns, Smith & Hamilton 2008), release freshwater into the ocean (Fricker et al. 2007), deform glacial landforms (Lewis et al. 2006), and disturb subglacial habitats (Siegert et al. 2005). Although the surface expression of sub-glacial lake drainage has been recorded in pulse-limited (Wingham et al. 2006b) and laser (Fricker et al. 2007) altimetry, conventional measurements acquired at the POCA have been shown to preferentially sample the highest sections of surface depressions (McMillan et al. 2013). A consequence is that POCA tends to underestimate the deflation. For example, estimates of the volume change within depressions above presumed sub-glacial lake sites in the Thwaites Glacier catchment (Figure 14) based on POCA L2swath elevation data differ by more than 40%. L2swath resolves this problem, and will lead to an improved inventory of active sub-glacial lakes (Smith et al. 2009, Wright, Siegert 2012) and their water mass budgets. In Greenland and on the Antarctic Peninsula, supra-glacial lakes similarly create and occupy depressions on the ice sheet surface (Liestl, Repp & Wold 1980, Scambos et al. 2000, McMillan et al. 2007), and the ability to map their shape in full (Ignéczi et al. 2016) will lead to an improved characterisation of their

seasonal hydrology which is believed to influence rates of ice flow (Das et al. 2008) and ice shelf stability (Phillips, Rajaram & Steffen 2010).

6. Conclusions

Trends in the elevation of ice sheets, ice caps, and mountain glaciers derived from satellite altimetry are a key observation for quantifying and understanding the impacts of environmental change. We have described how swath interferometric processing of CryoSat-2 data provides a step change in the quantity of valid elevation data that can be derived from satellite radar altimetry. By applying the technique to CryoSat-2 measurements acquired over a range of geophysical targets, we demonstrate that a tenfold gain in the density of data can be achieved in comparison to conventional satellite altimetry performed only at the POCA. Furthermore, we show that the increase in data density is not detrimental to data quality, with only a modest (up to 50% and surface dependant) degradation in the bias and variability of elevation measurements relative to standard POCA approaches. L2swath also provide a near continuous elevation field, making it possible to form digital elevation models and to map rates of surface elevation change at a true resolution of 500 m - an order of magnitude finer than is the current state of the art for the continental ice sheets. This leads to a more accurate picture of the complexity of surface topography and patterns of surface elevation change within ice stream tributaries, along the ice sheet margins, ice shelves, and in surface depressions linked with ice sheet hydrology. Applied extensively, these new observations will transform our understanding of cryospheric change.

8. Acknowledgments

This work was supported by European Space Agency contracts CryoTop 4000107394/12/I-NB and CryoTop evolution 4000116874/16/I-NB (NG). The CryoSat-

2 satellite altimetry data are freely available from the European Space Agency (https://earth.esa.int/web/guest/data-access). The IceBridge airborne altimetry data are freely available from the National Snow and Ice Data Centre (https://nsidc.org/data/icebridge/). We are grateful to two anonymous reviewers and the editor, whose comments have significantly improved the manuscript

9. Figures and Tables

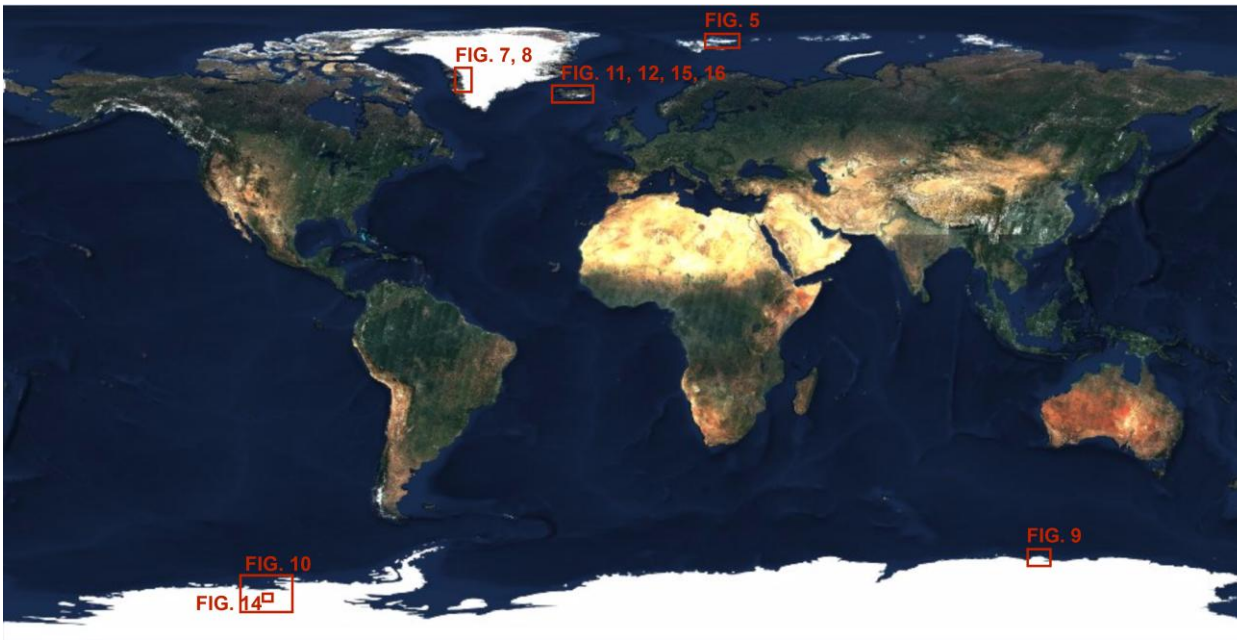

Figure 1: Map with figures location. Background is Sentinel-2 cloudless. Contains modified Copernicus Sentinel data 2016, EOX.

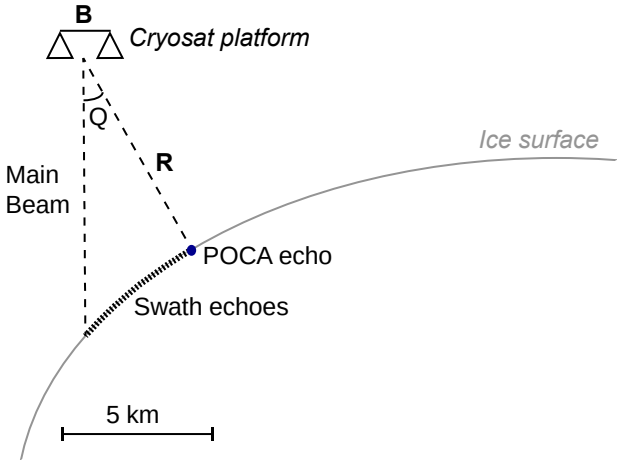

Figure 2: Swath interferometry retrieves elevation across the satellite ground track beyond the POCA. B is the interferometric baseline, R is the slant range, $\boldsymbol{\theta}$ is the look angle.

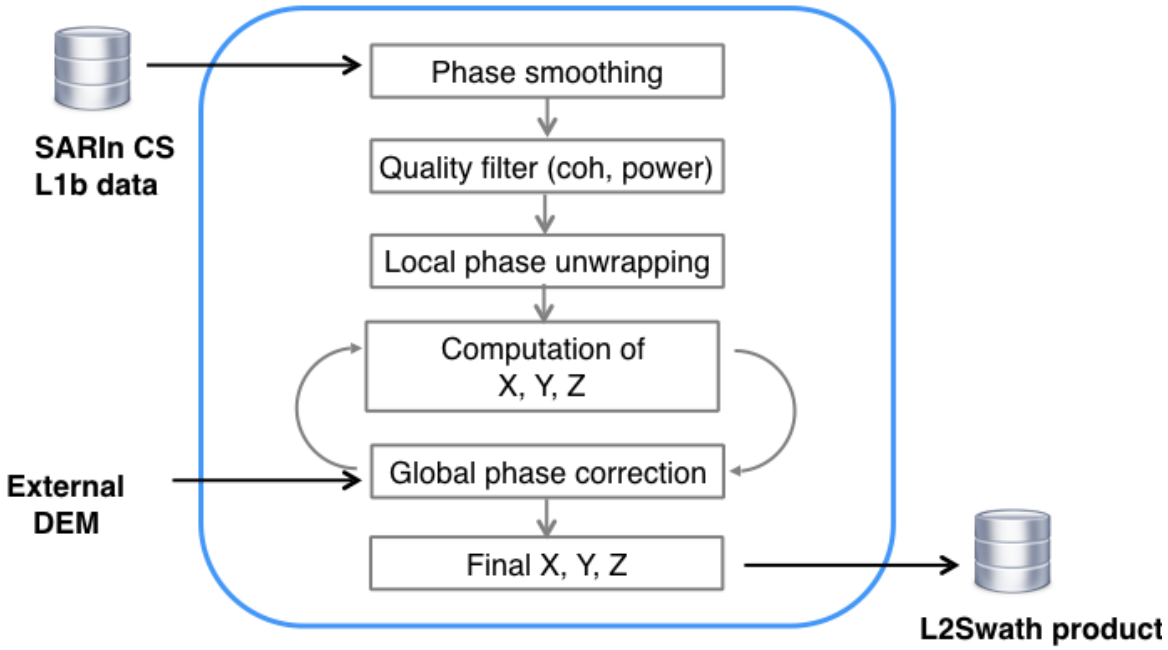

Figure 3: Swath processing workflow.

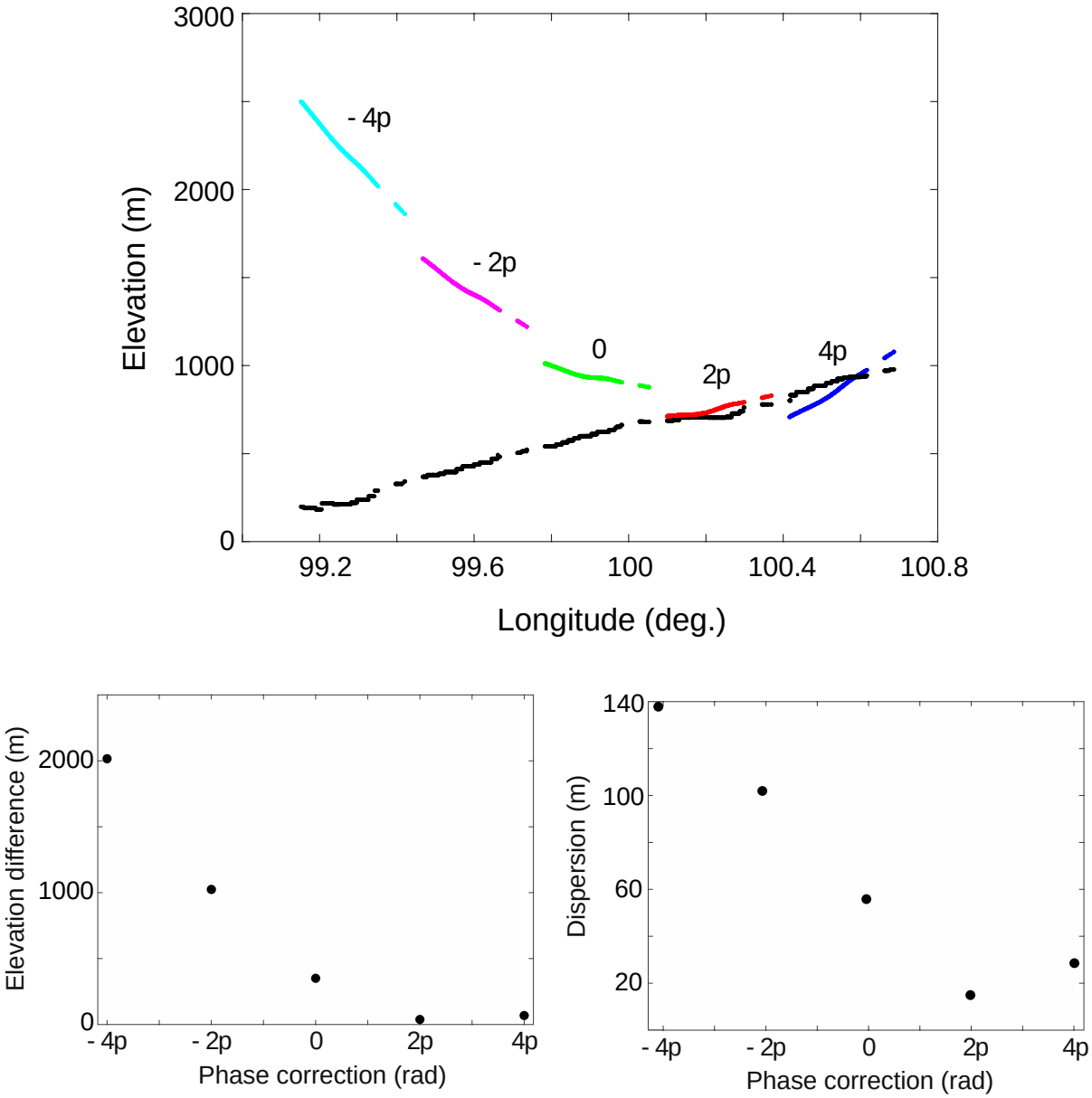

Figure 4: (top) Surface elevation of swath-processed CryoSat data to which 5 distinct values of phase ambiguity ([-4 -2 0 2 4]*π) have been applied and corresponding topography of the reference elevation dataset (black dots). Elevation difference (bottom left) and dispersion (bottom right) between swath-derived elevation and reference DEM_{ref} for various phase ambiguity. The correct phase ambiguity in this example is +2π.

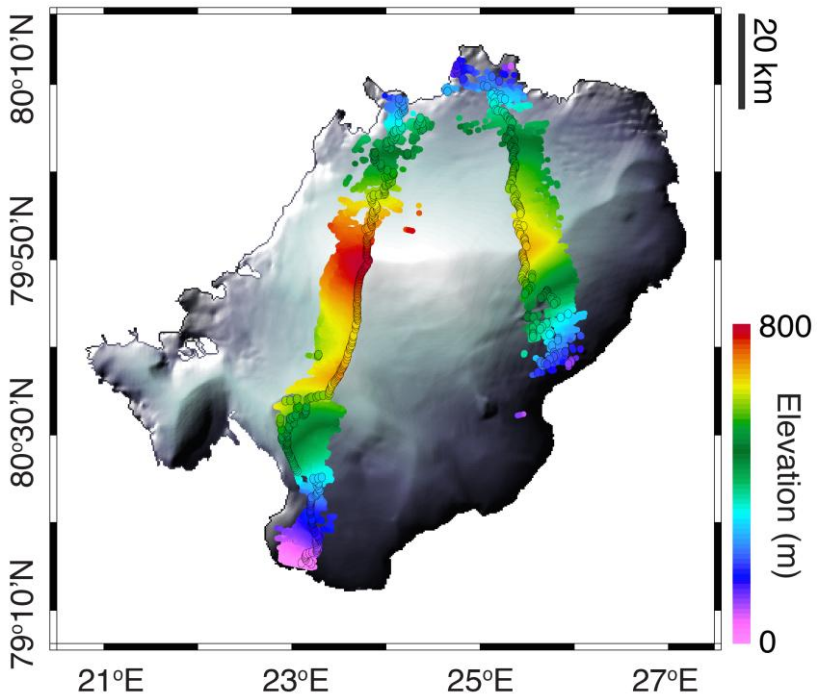

Figure 5: Austfonna ice cap, Svalbard, surface elevation determined using two orbits of swath (colour) and POCA (open circles) CryoSat-2 altimetry; swath altimetry delivers a 75-fold increase in spatial sampling.

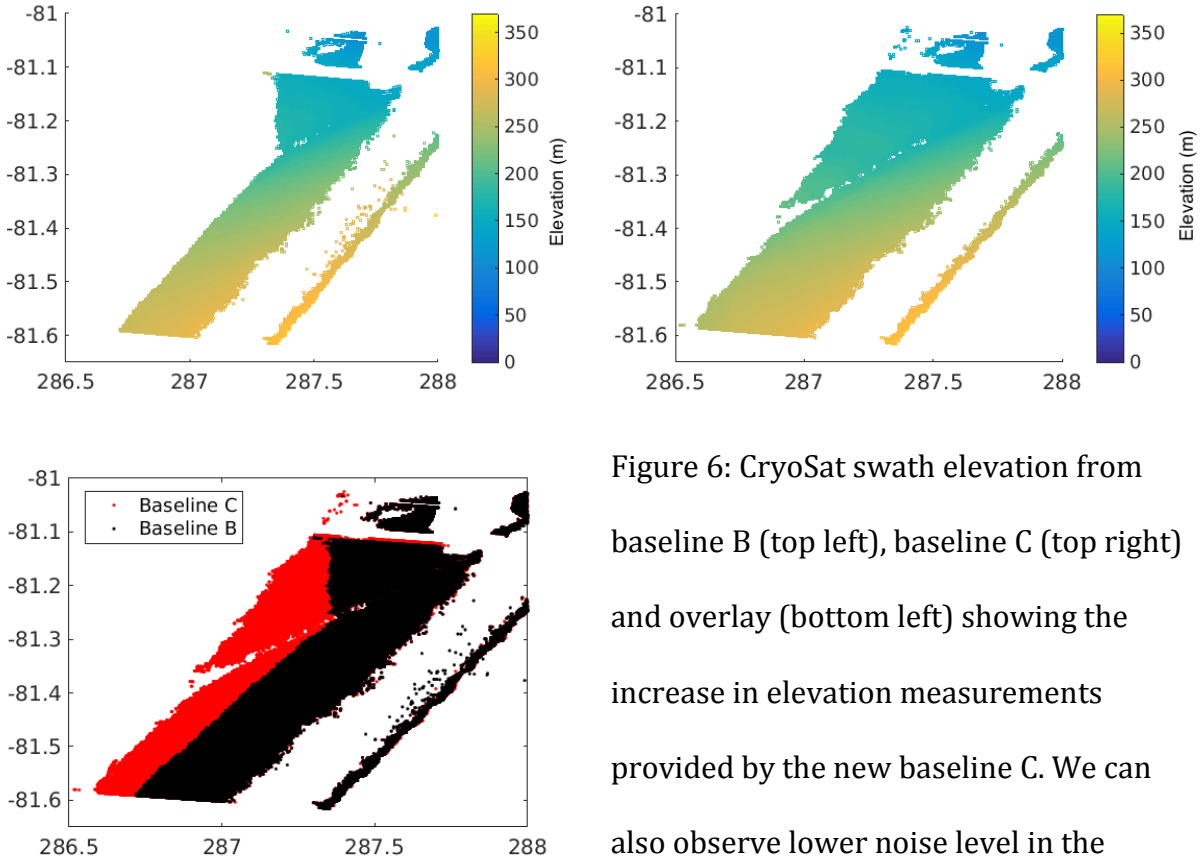

Figure 6: CryoSat swath elevation from baseline B (top left), baseline C (top right) and overlay (bottom left) showing the increase in elevation measurements provided by the new baseline C. We can also observe lower noise level in the baseline C product near the waveform's leading edge (top) as described by (Scagliola, Fornari 2015).

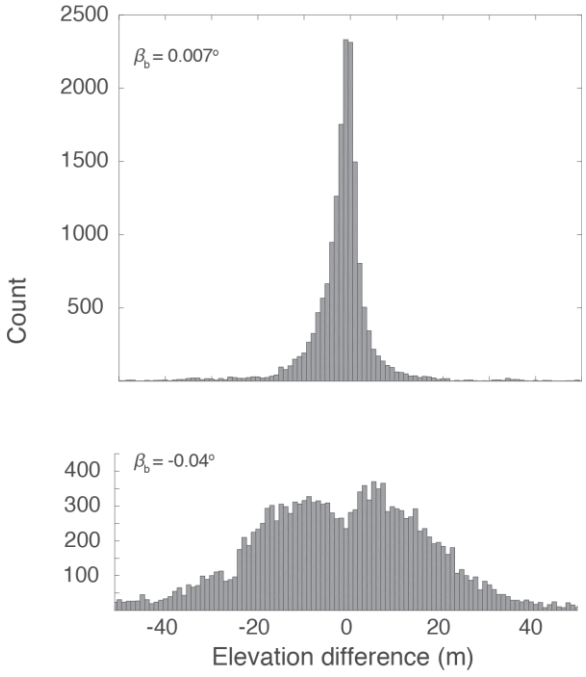

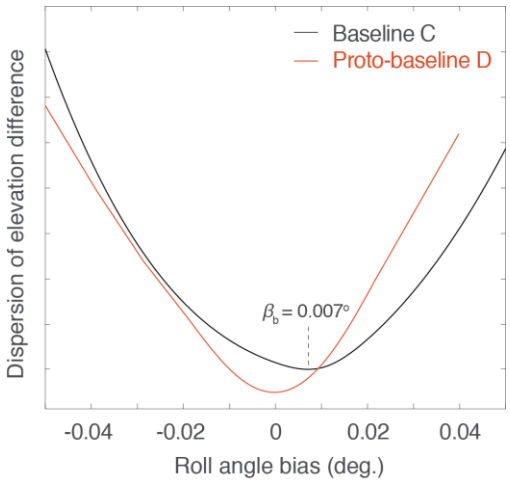

Figure 7: Distribution of 39139 L2swath elevation minus OIB elevation over the Jakobshavn area (Figure 8) with respect to experimental roll angle bias β_b = 0.007° and -0.04° (left). The roll bias that minimises the dispersion of the elevation difference is found at β_b = 0.007° (right). The same exercise using recently released corrected attitude information (Proto-baseline D data) shows that the roll angle is significantly improved (right).

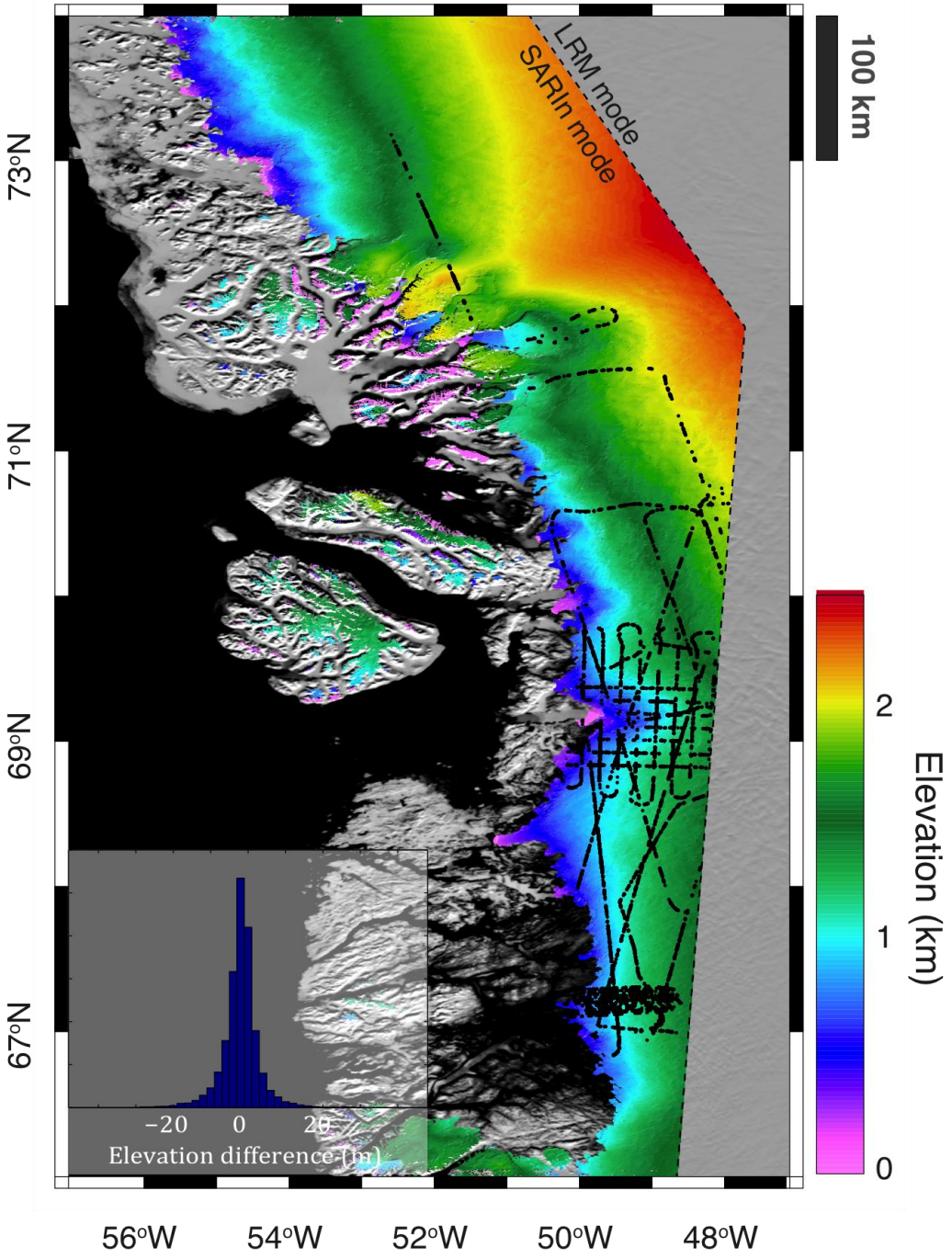

Figure 8: CryoTop L2swath continuous elevation at 500 m posting along the west coast of the GrIS overlaid over the MEaSUREs MODIS Mosaic of Greenland (Haran et al. 2013). The inland limit of the L2swath DEM corresponds to the CryoSat-2's SARIn mode mask (dashed line), elsewhere the ice mask is according to the GIMP dataset (Howat, Negrete & Smith 2014). IceBridge elevation acquired in March, April and May 2011 (black) and elevation difference with L2swath elevation for 39139 collocated measurements (inset).

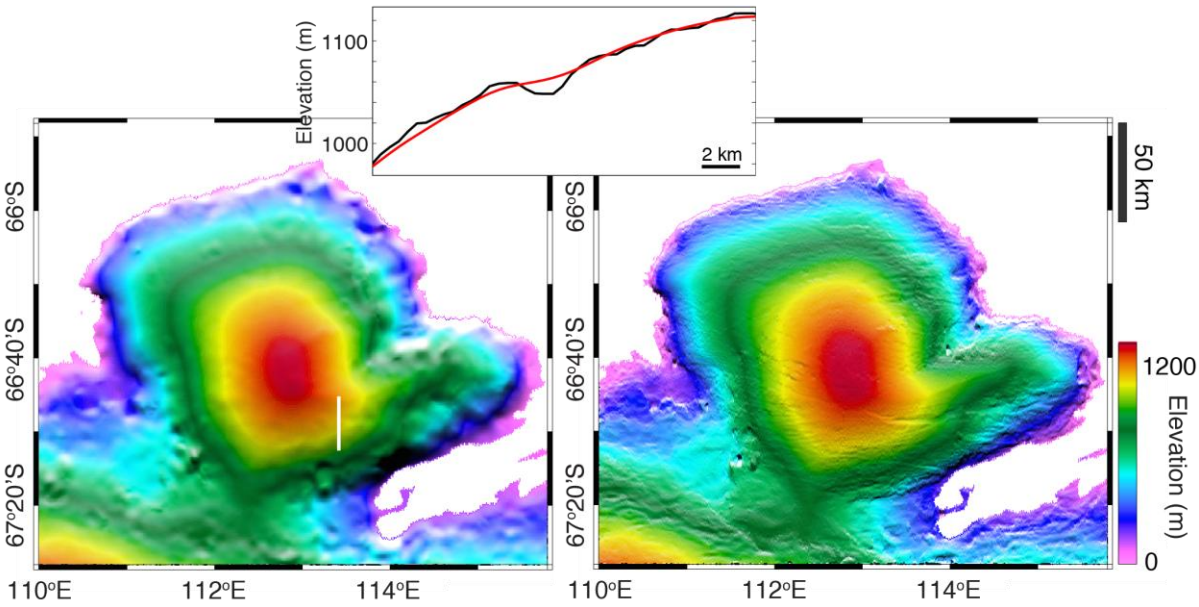

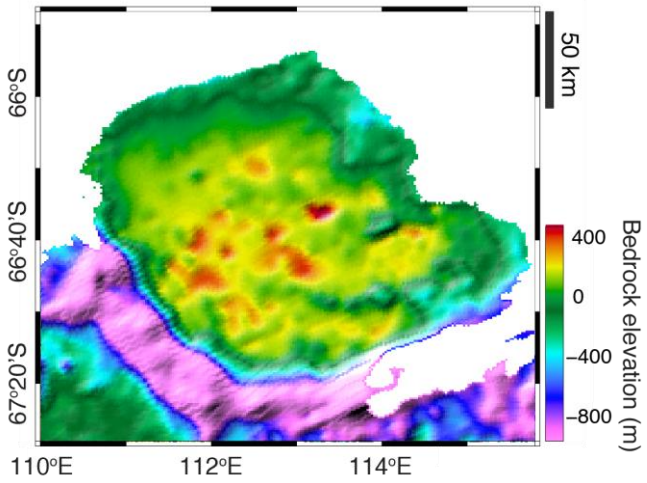

Figure 9: A continuous digital elevation model of the Law Dome, East Antarctica, (top left) from Bedmap2 posted at 1000m grid spacing (Fretwell et al. 2013), (top right) from swath mode interferometry posted at 500 m grid spacing and precise to within 2 metres. A profile (white line) shows example of small-scale features imaged by high resolution. Bedrock elevation is also shown (bottom left) (Fretwell et al. 2013).

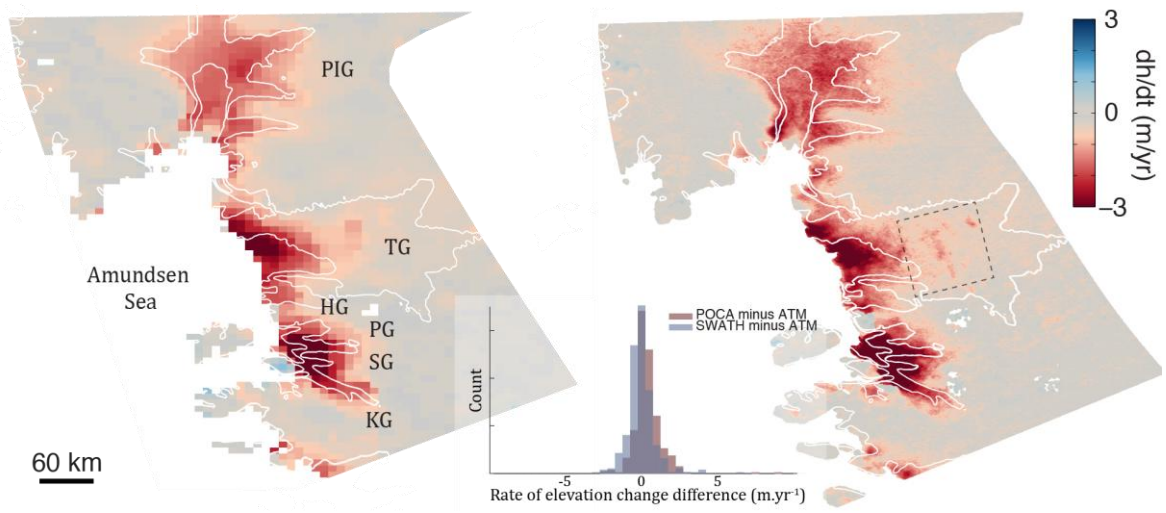

Figure 10: Surface elevation change over the Amundsen Sea Sector (left) mapped, continuously, with 10km grid spacing; (right) mapped, continuously, with 500 metre grid spacing (10 times finer than previous assessments) and an estimated precision of 0.2 m a^{-1}. Named glaciers are Pine Island (PIG), Thwaites (TG), Haynes (HG), Pope (PG), Smith (SG), Kohler (KG), the dashed area is the location of sub-glacial lakes (Figure 14). The mean difference between swath-derived rates of elevation change and airborne measurement is 0.04 ± 0.92 m a^{-1}, for comparison, the difference between POCA-derived rates of elevation change and airborne measurement is 0.40 ± 0.95 m a^{-1} (McMillan et al. 2014b).

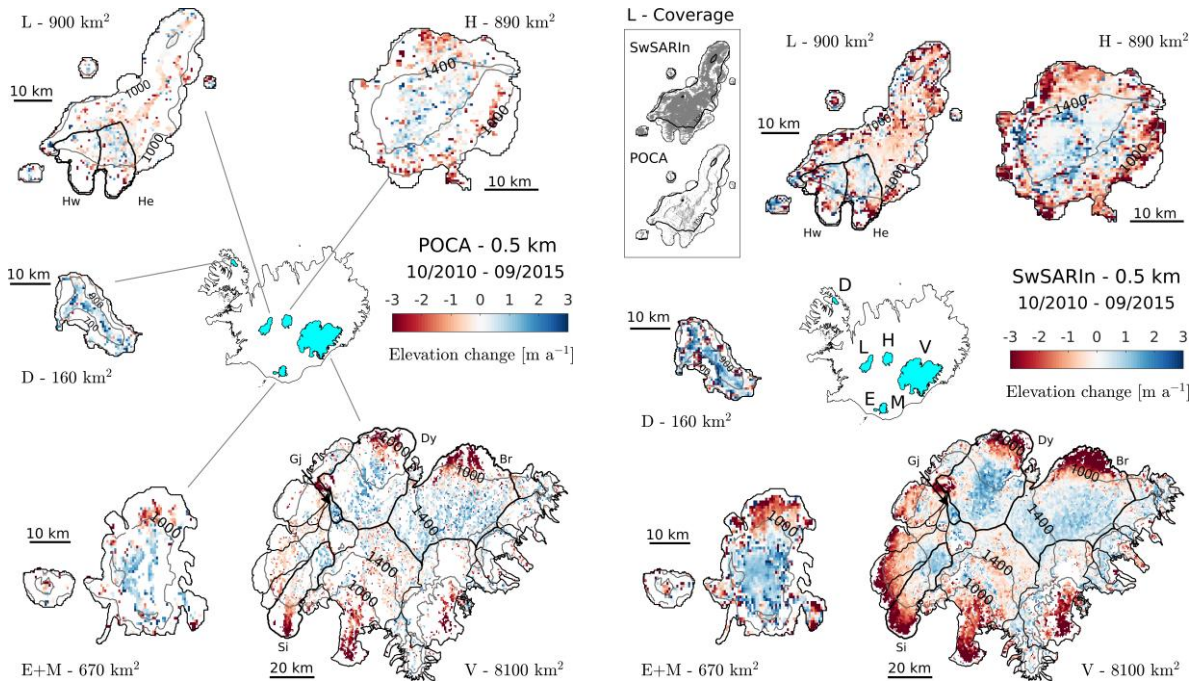

Figure 11: Rates of surface elevation for Icelandic ice caps determined from POCA (left) and L2swath (right) (Foresta et al. 2016). Relative density of elevation data determined via POCA and L2swath techniques for the Langjokull ice cap is shown in the inset (right).

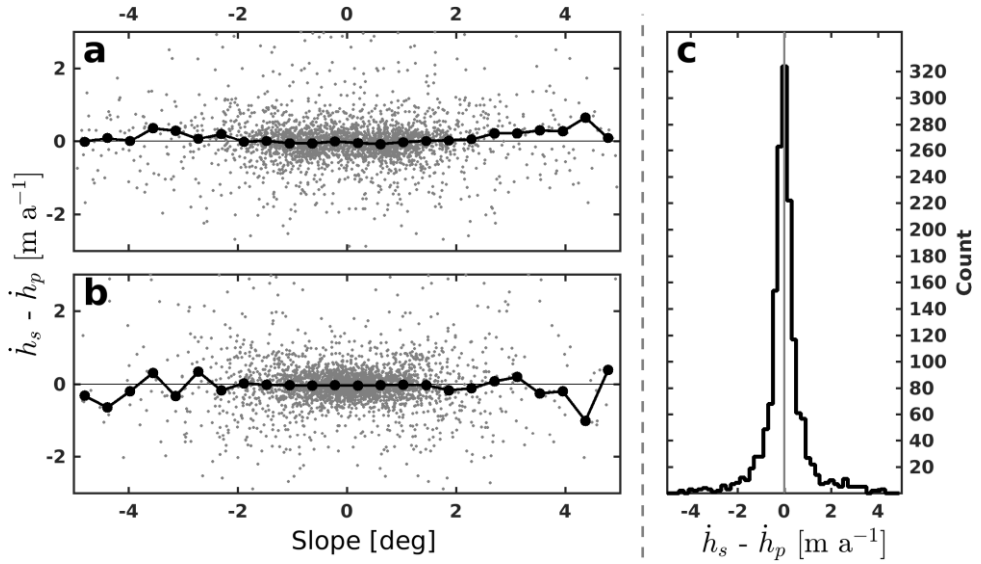

Figure 12: Difference between L2swath and POCA surface elevation change rates ($\dot{\boldsymbol{h}}_{\boldsymbol{s}} - \dot{\boldsymbol{h}}_{\boldsymbol{p}}$) over Vatnajökull with respect to (a) along-track and (b) across-track surface slope. (c) Histogram of differences between L2swath and POCA rates of surface elevation change (Foresta et al. 2016).

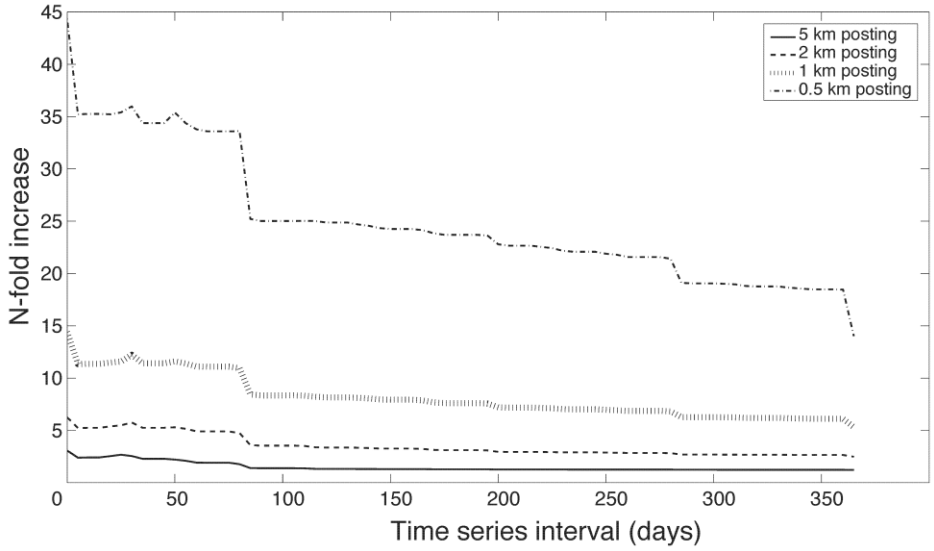

Figure 13: Increase in temporal resolution from conventional POCA to L2swath as a function of time interval and spatial posting. This has been calculated from real data over the Jakobshavn and Amundsen Sea sector areas.

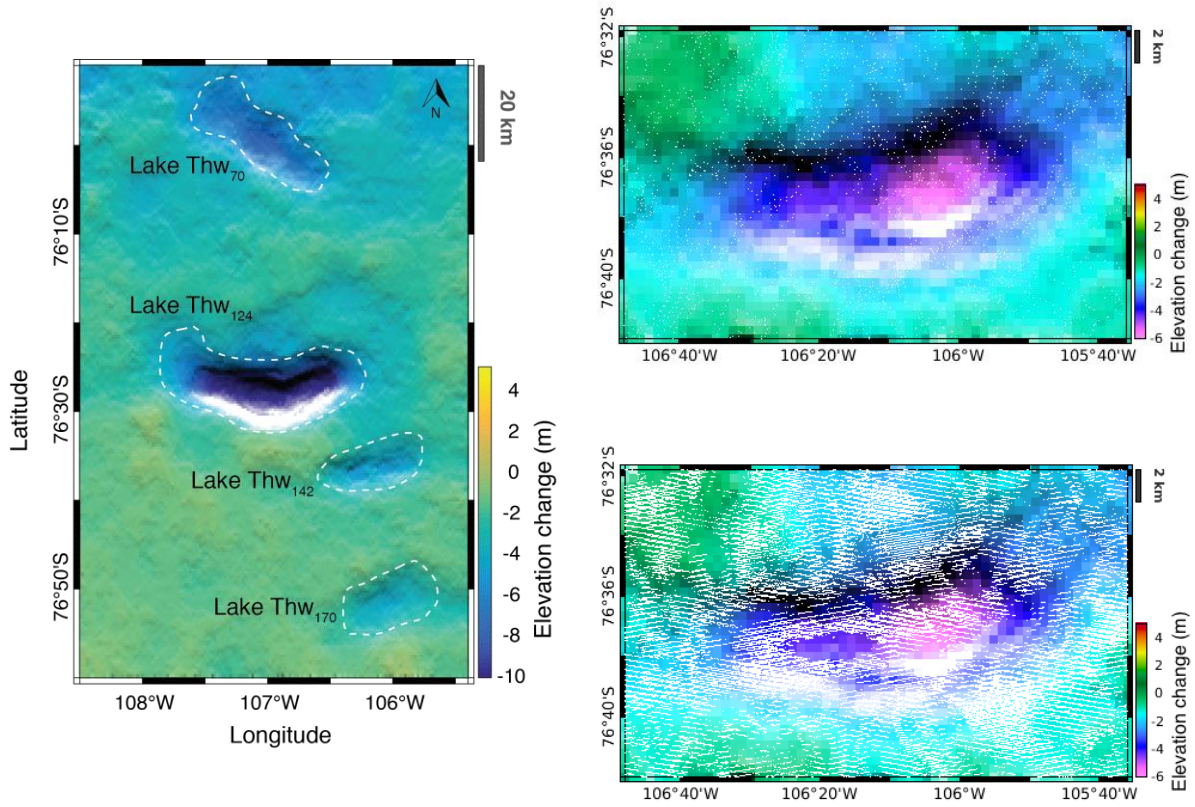

Figure 14: Surface elevation change between pre and post summer 2013 inland of the Thwaites glacier (location in Figure 10) from L2swath, showing areas of surface lowering related to the drainage of 4 subglacial lakes in mid 2013 (Smith et al. 2016). Zoom on lake Thw_{142} showing the location of all measurements (white dots) acquired over a CryoSat-2 repeat cycle from POCA (top right) and from L2swath (bottom right);

background image is L2swath derived surface elevation change in both cases.

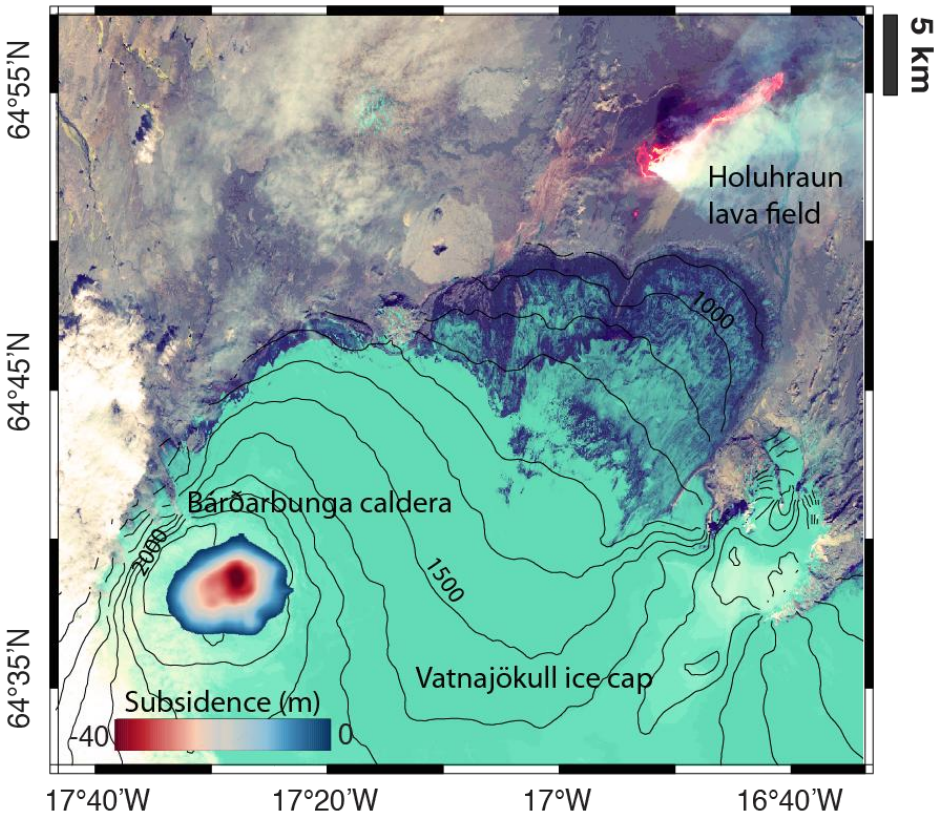

Figure 15: Rapid subsidence of the 4 km wide Bárðarbunga caldera, Vatnajökull ice cap, Iceland, after deflation of the magma chamber. Landsat-8 background image (September 6, 2014) shows contemporary Holuhraun lava flow. Elevation shown as 100 m equidistant contour lines.

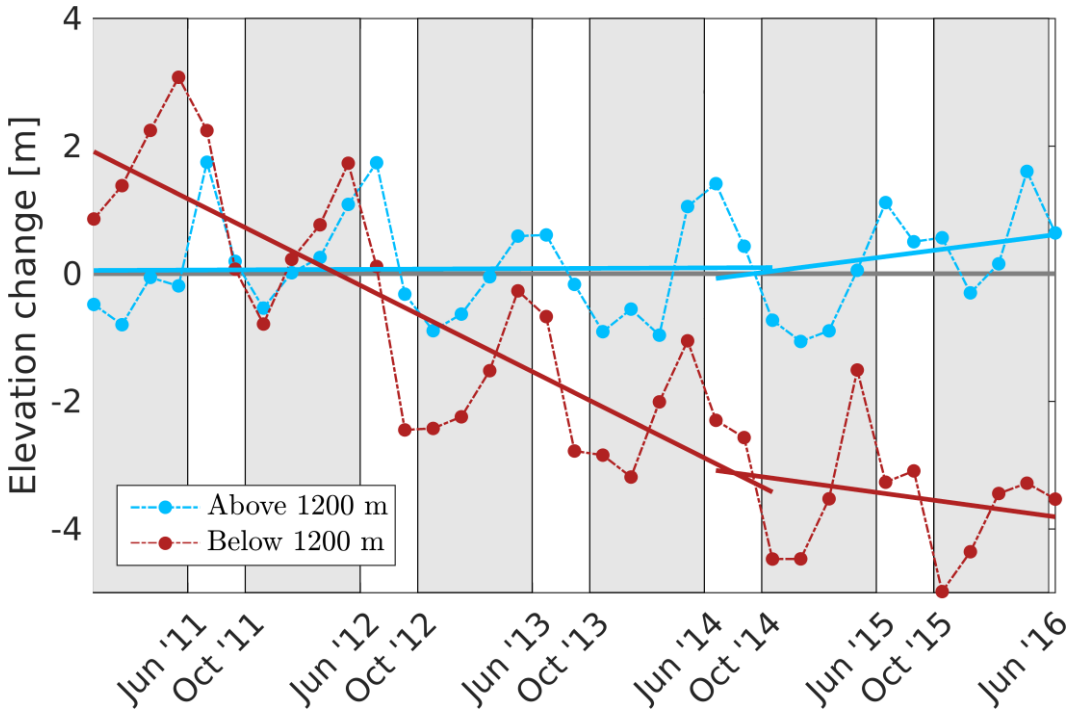

Figure 16: Vatnajökull elevation time series (60 days step) produced from L2swath elevations above and below 1200 m, used as an approximate ice cap wide ELA. The dark grey bands highlight the accumulation period between October and May; the nonshaded area corresponds to the ablation period between June and September. The two trends show mean rates of elevation change between 2010–2014 and between 2014–2016 (Foresta et al. 2016).

Table 1: Bias and dispersion of swath mode elevation and derived gridded products, POCA, with respect to Operation IceBridge Airborne Laser Scanner and comparative measurements density between POCA and swath mode

Region	Swath elevation (m)	POCA elevation (m)	Swath/POCA Number of measures (10^3)	Gain in spatial resolution	Swath DEM (m)	Swath dh/dt ($m.a^{-1}$)	POCA dh/dt ($m.a^{-1}$)
Petermann	-1.3±1.2	-1.1±0.8	44.9/1.4	5 folds	NA	NA	NA
Jakobshavn	-1.2±2.0	-0.6±1.4	99.9/1.0	10 folds	-1.4±1.8	0.04±1.15	0.17±1.54
Amundsen Sea Sector	-2.0±2.0	-1.1±1.3	199.3/3.3	8 folds	-1.7±2.0	0.04±0.92	0.40±0.95

Bamber, J.L., Gomez-Dans, J.L. & Griggs, J.A. 2009, "A new 1 km digital elevation model of the Antarctic derived from combined satellite radar and laser data, Part 1: Data and methods", *The Cryosphere,* vol. 3, no. 1, pp. 101-111.

Bamber, J.L., Griggs, J.A., Hurkmans, R.T.W.L., Dowdeswell, J.A., Gogineni, S.P., Howat, I., Mouginot, J., Paden, J., Palmer, S., Rignot, E. & Steinhage, D. 2013, "A new bed elevation dataset for Greenland", *The Cryosphere,* vol. 7, no. 2, pp. 499-510.

Berthier, E., Vincent, C., Magnússon, E., Gunnlaugsson, Á.Þ., Pitte, P., Le Meur, E., Masiokas, M., Ruiz, L., Pálsson, F., Belart, J.M.C. & Wagnon, P. 2014, "Glacier topography and elevation changes derived from Pléiades sub-meter stereo images", *The Cryosphere,* vol. 8, no. 6, pp. 2275-2291.

Brenner, A.C., Blndschadler, R.A., Thomas, R.H. & Zwally, H.J. 1983, "Slope-induced errors in radar altimetry over continental ice sheets", *Journal of Geophysical Research: Oceans,* vol. 88, no. C3, pp. 1617-1623.

Christie, F.D.W., Bingham, R.G., Gourmelen, N., Tett, S.F.B. & Muto, A. 2016, "Four-decade record of pervasive grounding line retreat along the Bellingshausen margin of West Antarctica", *Geophysical Research Letters,* vol. 43, no. 11, pp. 5741-5749.

Das, S.B., Joughin, I., Behn, M.D., Howat, I.M., King, M.A., Lizarralde, D. & Bhatia, M.P. 2008, "Fracture propagation to the base of the Greenland Ice Sheet during supraglacial lake drainage", *Science,* vol. 320, no. 5877, pp. 778-781.

Dehecq, A., Gourmelen, N., Shepherd, A., Cullen, R. & Trouvé, E. 2013, "Evaluation of CryoSat-2 for height retrieval over the Himalayan range", *CryoSat-2 third user workshop*.

Dehecq, A., Millan, R., Berthier, E., Gourmelen, N., Trouvé, E. & Vionnet, V., 2016, "Elevation Changes Inferred From TanDEM-X Data Over the Mont-Blanc Area: Impact of the X-Band Interferometric Bias", *IEEE Journal of Selected Topics in Applied Earth Observations and Remote Sensing,* vol. 9, no. 8, pp. 3870-3882.

DiMarzio, J., Brenner, A., Schutz, R., Shuman, C.A. & Zwally, H.J. 2007a, *GLAS/ICESat 1 km laser altimetry digital elevation model of Greenland*, National Snow and Ice Data Center, Boulder, Colorado, USA. https://nsidc.org/data/nsidc-0305

DiMarzio, J., Brenner, A., Schutz, R., Shuman, C.A. & Zwally, H.J. 2007b, *GLAS/ICESat 500 m laser altimetry digital elevation model of Antarctica*, National Snow and Ice Data Center, Boulder, Colorado, USA. https://nsidc.org/data/nsidc-0304

Drinkwater, M.R., Ratier, G., Wingham, D. & Francis, R. 2005, "The European Space Agency's Earth Explorer Mission CryoSat: Measuring Variability in the Cryosphere", *Annals of Glaciology,* vol. 39, pp. 313-320.

Foresta, L., Gourmelen, N., Pálsson, F., Nienow, P., Björnsson, H. & Shepherd, A. 2016, "Surface elevation change and mass balance of Icelandic ice caps derived from swath mode CryoSat-2 altimetry", *Geophysical Research Letters,* vol. 43, no. 23, pp. 12,138-12,145.

Fretwell, P., Pritchard, H.D., Vaughan, D.G., Bamber, J.L., Barrand, N.E., Bell, R., Bianchi, C., Bingham, R.G., Blankenship, D.D., Casassa, G., Catania, G., Callens, D., Conway, H., Cook, A.J., Corr, H.F.J., Damaske, D., Damm, V., Ferraccioli, F., Forsberg, R., Fujita, S., Gim, Y., Gogineni, P., Griggs, J.A., Hindmarsh, R.C.A., Holmlund, P., Holt, J.W., Jacobel, R.W., Jenkins, A., Jokat, W., Jordan, T., King, E.C., Kohler, J., Krabill, W., Riger-Kusk, M., Langley, K.A., Leitchenkov, G., Leuschen, C., Luyendyk, B.P., Matsuoka, K., Mouginot, J., Nitsche, F.O., Nogi, Y., Nost, O.A., Popov, S.V., Rignot, E., Rippin, D.M., Rivera, A., Roberts, J., Ross, N., Siegert, M.J., Smith, A.M., Steinhage, D., Studinger, M., Sun, B., Tinto, B.K., Welch, B.C., Wilson, D., Young, D.A., Xiangbin, C. & Zirizzotti, A. 2013,

"Bedmap2: improved ice bed, surface and thickness datasets for Antarctica", *The Cryosphere,* vol. 7, no. 1, pp. 375-393.

Fricker, H.A., Scambos, T., Bindschadler, R. & Padman, L. 2007, "An active subglacial water system in West Antarctica mapped from space", *Science,* vol. 315, no. 5818, pp. 1544-1548.

Garcia-Mondejar, A., M. Fornari, M. Roca (2017) CryoSat-2: SIRAL Calibration with Transponders, *Cryosat-2 Advances in Space Science*, This issue.

Gardner, A.S., Moholdt, G., Cogley, J.G., Wouters, B., Arendt, A.A., Wahr, J., Berthier, E., Hock, R., Pfeffer, W.T., Kaser, G., Ligtenberg, S.R.M., Bolch, T., Sharp, M.J., Hagen, J.O., van den Broeke, M.R. & Paul, F. 2013, "A Reconciled Estimate of Glacier Contributions to Sea Level Rise: 2003 to 2009", *Science,* vol. 340, no. 6134, pp. 852-857.

Gourmelen, N., Goldberg, D., Snow, K., Henley, S., Bingham, R., Kimura, S., Hogg, A., Shepherd, A., Mouginot, J., Lenearts, J., Ligtenberg, S. & van de Berg, W. 2017, "Channelized melting drives thinning under a rapidly melting Antarctic ice shelf", *Geophysical Research Letters,* 44, 9796–9804. 10.1002/2017GL074929.

Gray, L., Burgess, D., Copland, L., Cullen, R., Galin, N., Hawley, R. & Helm, V. 2013, "Interferometric swath processing of Cryosat-2 data for glacial ice topography", *The Cryosphere Discussions,* vol. 7, no. 3, pp. 3133-3162.

Gray, L., Burgess, D., Copland, L., Demuth, M.N., Dunse, T., Langley, K. & Schuler, T.V. 2015, "CryoSat-2 delivers monthly and inter-annual surface elevation change for Arctic ice caps", *The Cryosphere,* vol. 9, no. 5, pp. 1895-1913.

Gray, L., Burgess, D., Copland, L., Dunse, T., Langley, K. & Moholdt, G. 2016, "Improved processing and calibration of the interferometric mode of the CryoSat radar altimeter allows height measurements of supraglacial lakes in west Greenland", *The Cryosphere Discussions,* vol. 2016, pp. 1-38.

Griggs, J.A. & Bamber, J.L. 2009, "A new 1 km digital elevation model of Antarctica derived from combined radar and laser data, Part 2: Validation and error estimates", *The Cryosphere,* vol. 3, no. 1, pp. 113-123.

Haran, T., Bohlander, J., Scambos, T., Painter, T. & Fahnestock, M. 2013, "*MEaSUREs MODIS Mosaic of Greenland 2005 (MOG2005) Image Map, Version 1*. Boulder, Colorado USA. NSIDC: National Snow and Ice Data Center." nsidc.org/data/nsidc-0547.

Hawley, R.L., Shepherd, A., Cullen, R., Helm, V. & Wingham, D.J. 2009, "Ice-sheet elevations from across-track processing of airborne interferometric radar altimetry", *Geophysical Research Letters,* vol. 36, no. 22, pp. L22501.

Howat, I.M., Negrete, A. & Smith, B.E. 2014, "The Greenland Ice Mapping Project (GIMP) land classification and surface elevation datasets", *The Cryosphere Discussions,* vol. 8, no. 1, pp. 453-478.

Howat, I.M., Porter, C., Noh, M.J., Smith, B.E. & Jeong, S. 2015, "Brief Communication: Sudden drainage of a subglacial lake beneath the Greenland Ice Sheet", *The Cryosphere,* vol. 9, no. 1, pp. 103-108.

Ignéczi, Á., Sole, A.J., Livingstone, S.J., Leeson, A., Fettweis, X., Selmes, N., Gourmelen, N. & Briggs, K. 2016, "North-east sector of the Greenland Ice Sheet to undergo the greatest inland expansion of supraglacial lakes during the 21st century", *Geophysical Research Letters,* 43, 9729–9738, doi:10.1002/2016GL070338.

IPCC, 2013: *Climate Change 2013: The Physical Science Basis. Contribution of Working Group I to the Fifth Assessment Report of the Intergovernmental Panel on Climate Change* [Stocker, T.F., D. Qin, G.-K. Plattner, M. Tignor, S.K. Allen, J. Boschung, A.

Nauels, Y. Xia, V. Bex and P.M. Midgley (eds.)]. Cambridge University Press, Cambridge, United Kingdom and New York, NY, USA, 1535 pp, doi:10.1017/CBO9781107415324.

Joughin, I., Tulaczyk, S., Fahnestock, M. & Kwok, R. 1996, "A Mini-Surge on the Ryder Glacier, Greenland, Observed by Satellite Radar Interferometry", *Science,* vol. 274, no. 5285, pp. 228-230.

Kaab, A., Berthier, E., Nuth, C., Gardelle, J. & Arnaud, Y. 2012, "Contrasting patterns of early twenty-first-century glacier mass change in the Himalayas", *Nature,* vol. 488, no. 7412, pp. 495-498.

Krabill, W.B. 2016, "*IceBridge ATM L2 Icessn Elevation, Slope, and Roughness, Version 2*. ", *Boulder, Colorado USA. NASA National Snow and Ice Data Center Distributed Active Archive Center*. http://nsidc.org/data/ilatm2

Krabill, W.B. 2015, *IceBridge ATM L4 Surface Elevation Rate of Change*, NASA National Snow and Ice Data Center Distributed Active Archive Center., Boulder Colorado, USA. https://nsidc.org/data/IDHDT4

Lewis, A.R., Marchant, D.R., Kowalewski, D.E., Baldwin, S.L. & Webb, L.E. 2006, "The age and origin of the Labyrinth, western Dry Valleys, Antarctica: Evidence for extensive middle Miocene subglacial floods and freshwater discharge to the Southern Ocean", *Geology,* vol. 34, no. 7, pp. 513-516.

Liestl, O., Repp, K. & Wold, B. 1980, "Supra-glacial lakes in Spitsbergen", *Norsk Geografisk Tidsskrift,* vol. 34, pp. 89-92.

Martin, C.F., Krabill, W.B., Manizade, S.S., Russell, R.L., Sonntag, J.G., Swift, R.N. & Yungel, J.K. 2012, *Airborne topographic mapper calibration procedures and accuracy assessment,* Greenbelt, Md.: National Aeronautics and Space Administration, Goddard Space Flight Center, 2012, NASA/TM-2012-215891.

McMillan, M., Corr, H., Shepherd, A., Ridout, A., Laxon, S. & Cullen, R. 2013, "Three-dimensional mapping by CryoSat-2 of subglacial lake volume changes", *Geophysical Research Letters,* vol. 40, no. 16, pp. 4321-4327.

McMillan, M., Leeson, A., Shepherd, A., Briggs, K., Armitage, T.W.K., Hogg, A., Munneke, P.K., van den Broeke, M., Brice, N., van de Berg, W.J., Ligtenberg, S., Horwath, M., Groh, A., Muir, A. & Gilbert, L. 2016, "A high resolution record of Greenland mass balance", *Geophysical Research Letters,* 43, 7002–7010, doi:10.1002/2016GL069666.

McMillan, M., Nienow, P., Shepherd, A., Benham, T. & Sole, A. 2007, "Seasonal evolution of supra-glacial lakes on the Greenland Ice Sheet", *Earth and Planetary Science Letters,* vol. 262, no. 3-4, pp. 484-492.

McMillan, M., Shepherd, A., Gourmelen, N., Dehecq, A., Leeson, A., Ridout, A., Flament, T., Hogg, A., Gilbert, L., Benham, T., van den Broeke, M., Dowdeswell, J.A., Fettweis, X., Noël, B. & Strozzi, T. 2014a, "Rapid dynamic activation of a marine-based Arctic ice cap", *Geophysical Research Letters,* 41, 8902–8909, doi:10.1002/2014GL062255.

McMillan, M., Shepherd, A., Sundal, A., Briggs, K., Muir, A., Ridout, A., Hogg, A. & Wingham, D. 2014b, "Increased ice losses from Antarctica detected by CryoSat-2", *Geophysical Research Letters,* vol. 41, no. 11, pp. 3899-3905.

Phillips, T., Rajaram, H. & Steffen, K. 2010, "Cryo-hydrologic warming: A potential mechanism for rapid thermal response of ice sheets", *Geophysical Research Letters,* vol. 37, no. 20, L20503.

Pritchard, H.D., Arthern, R.J., Vaughan, D.G. & Edwards, L.A. 2009, "Extensive dynamic thinning on the margins of the Greenland and Antarctic ice sheets", *Nature,* vol. 461, no. 7266, pp. 971-975.

Reykjavik Institute of Earth Sciences, *Bárðarbunga subsidence*. Available: http://en.vedur.is/earthquakes-and-volcanism/articles/nr/3023.

Scagliola, M. & Fornari, M. 2015, *Main evolutions and expected quality improvements in BaselineC Level1b products*, no. 1.3, C2-TN-ARS-GS-5154.

Scambos, T.A., Hulbe, C., Fahnestock, M. & Bohlander, J. 2000, "The link between climate warming and break up of ice shelves in the Antarctic Peninsula", *Journal of Glaciology,* vol. 46, no. 154, pp. 516-530.

Schenk, T., Csatho, B. & Lee, D.C. 1999, "Quality control issues of airborne laser ranging data and accuracy study in an urban area ", *IAPRS*, La Jolla, California, Vol. 32, Part 3W14, 8 pages.

Shepherd, A., Wingham, D., Payne, T. & Skvarca, P. 2003, "Larsen ice shelf has progressively thinned", *Science,* vol. 302, no. 5646, pp. 856-859.

Shepherd, A., Wingham, D.J., Mansley, J.A.D. & Corr, H.F.J. 2001, "Inland thinning of Pine Island Glacier, West Antarctica", *Science,* vol. 291, no. 5505, pp. 862-864.

Shepherd, A., Ivins, E.R., A, G., Barletta, V.R., Bentley, M.J., Bettadpur, S., Briggs, K.H., Bromwich, D.H., Forsberg, R., Galin, N., Horwath, M., Jacobs, S., Joughin, I., King, M.A., Lenaerts, J.T.M., Li, J., Ligtenberg, S.R.M., Luckman, A., Luthcke, S.B., McMillan, M., Meister, R., Milne, G., Mouginot, J., Muir, A., Nicolas, J.P., Paden, J., Payne, A.J., Pritchard, H., Rignot, E., Rott, H., Sørensen, L.S., Scambos, T.A., Scheuchl, B., Schrama, E.J.O., Smith, B., Sundal, A.V., van Angelen, J.H., van de Berg, W.J., van den Broeke, M.R., Vaughan, D.G., Velicogna, I., Wahr, J., Whitehouse, P.L., Wingham, D.J., Yi, D., Young, D. & Zwally, H.J. 2012, "A Reconciled Estimate of Ice-Sheet Mass Balance", *Science,* vol. 338, no. 6111, pp. 1183-1189.

Siegert, M.J., Carter, S., Tabacco, I., Popov, S. & Blankenship, D.D. 2005, "A revised inventory of Antarctic subglacial lakes", *Antarctic Science,* vol. 17, no. 03, pp. 453-460.

Sigmundsson, F., Hooper, A., Hreinsdottir, S., Vogfjord, K.S., Ofeigsson, B.G., Heimisson, E.R., Dumont, S., Parks, M., Spaans, K., Gudmundsson, G.B., Drouin, V., Arnadottir, T., Jonsdottir, K., Gudmundsson, M.T., Hognadottir, T., Fridriksdottir, H.M., Hensch, M., Einarsson, P., Magnusson, E., Samsonov, S., Brandsdottir, B., White, R.S., Agustsdottir, T., Greenfield, T., Green, R.G., Hjartardottir, A.R., Pedersen, R., Bennett, R.A., Geirsson, H., La Femina, P.C., Bjornsson, H., Palsson, F., Sturkell, E., Bean, C.J., Mollhoff, M., Braiden, A.K. & Eibl, E.P.S. 2015, "Segmented lateral dyke growth in a rifting event at Bareth]arbunga volcanic system, Iceland", *Nature,* vol. 517, no. 7533, pp. 191-195.

Smith, B., E., Fricker, H.A., Joughin, I.R. & Tulaczyk, S. 2009, "An inventory of active subglacial lakes in Antarctica detected by ICESat (2003–2008)", *Journal of Glaciology,* vol. 55, no. 192, pp. 573-595.

Smith, B.E., Gourmelen, N., Huth, A. & Joughin, I. 2016, "Connected subglacial lake drainage beneath Thwaites Glacier, West Antarctica", *The Cryosphere Discussions,* vol. 2016, pp. 1-19.

Stearns, L.A., Smith, B.E. & Hamilton, G.S. 2008, "Increased flow speed on a large East Antarctic outlet glacier caused by subglacial floods", *Nature Geosci,* vol. 1, no. 12, pp. 827-831.

Wilson, W. S., Abdalati, W., Alsdorf, D., Benveniste, J., Bonekamp, H., Cogley, J. G., Drinkwater, M. R., Fu, L.-L., Gross, R., Haines, B. J., Harrison, D. E., Johnson, G. C., Johnson, M., LaBrecque, J. L., Lindstrom, E. J., Merrifield, M. A., Miller, L., Pavlis, E. C., Piotrowicz, S., Roemmich, D., Stammer, D., Thomas, R. H., Thouvenot, E. and Woodworth, P. L. 2010, “Observing Systems Needed to Address Sea-Level Rise and

Variability", in Understanding Sea-Level Rise and Variability (eds J. A. Church, P. L. Woodworth, T. Aarup and W. S. Wilson), Wiley-Blackwell, Oxford, UK. doi: 10.1002/9781444323276.ch12

Wingham, D.J., Francis, C.R., Baker, S., Bouzinac, C., Brockley, D., Cullen, R., de Chateau-Thierry, P., Laxon, S.W., Mallow, U., Mavrocordatos, C., Phalippou, L., Ratier, G., Rey, L., Rostan, F., Viau, P. & Wallis, D.W. 2006, "CryoSat: A mission to determine the fluctuations in Earth's land and marine ice fields", *Advances in Space Research*, 37, 841–871.

Wingham, D.J., Ridout, A., Scharroo, R., Arthern, R. & Shum, C.K. 1998, "Antarctic elevation change from 1992 to 1996", *Science,* vol. 282, no. 5388, pp. 456-458.

Wingham, D.J., Shepherd, A., Muir, A. & Marshall, G.J. 2006a, "Mass balance of the Antarctic ice sheet", *Philosophical Transactions of the Royal Society A-Mathematical Physical and Engineering Sciences,* vol. 364, no. 1844, pp. 1627-1635.

Wingham, D.J., Siegert, M.J., Shepherd, A. & Muir, A.S. 2006b, "Rapid discharge connects Antarctic subglacial lakes", *Nature,* vol. 440, no. 7087, pp. 1033-1036.

Wright, A. & Siegert, M. 2012, "A fourth inventory of Antarctic subglacial lakes", *Antarctic Science,* vol. 24, no. 06, pp. 659-664.

Zwally, H.J., Brenner, A.C., Major, J.A., Bindschadler, R.A. & Marsh, J.G. 1989, "Growth of Greenland Ice-Sheet - Measurement", *Science,* vol. 246, no. 4937, pp. 1587-1589.

Zwally, H.J., Giovinetto, M.B., Li, J., Cornejo, H.G., Beckley, M.A., Brenner, A.C., Saba, J.L. & Yi, D.H. 2005, "Mass changes of the Greenland and Antarctic ice sheets and shelves and contributions to sea-level rise: 1992-2002", *Journal of Glaciology,* vol. 51, no. 175, pp. 509-527.

***Detailed Response to Reviewers**

Click here to download Detailed Response to Reviewers: response2reviews_2.docx

Editor:

Editor's comments:

I have again reviewed the references and find the following need additional information. Once these references are complete the paper will be accepted.

Gourmelen, N., Goldberg, D., Snow, K., Henley, S., Bingham, R., Kimura, S., Hogg, A., Shepherd, A., Mouginot, J., Lenearts, J., Ligtenberg, S. & van de Berg, W. 2017, "Channelized melting drives thinning under a rapidly melting Antarctic ice shelf", Geophysical Research Letters, 10.1002/2017GL074929.

Volume number and inclusive page numbers are missing.

****

Ignéczi, Á., Sole, A.J., Livingstone, S.J., Leeson, A., Fettweis, X., Selmes, N., Gourmelen, N. & Briggs, K. 2016, "North-east sector of the Greenland Ice Sheet to undergo the greatest inland expansion of supraglacial lakes during the 21st century", Geophysical Research Letters, , pp. n/a-n/a.

Volume number and inclusive page numbers are missing.

****

IPCC 2013, Climate Change 2013 - The Physical Science Basis. Contribution of Working Group I to the Fifth Assessment Report of the IPCC, Cambridge University Press.

The publisher's city is missing.

****

Martin, C.F., Krabill, W.B., Manizade, S.S., Russell, R.L., Sonntag, J.G., Swift, R.N. & Yungel, J.K. 2012, Airborne topographic mapper calibration procedures and accuracy assessment, Greenbelt, Md.: National Aeronautics and Space Administration, Goddard Space Flight Center, 2012

The NASA technical report number should be cited. It is NASA/TM-2012-215891

****

McMillan, M., Leeson, A., Shepherd, A., Briggs, K., Armitage, T.W.K., Hogg, A., Munneke, P.K., van den Broeke, M., Brice, N., van de Berg, W.J., Ligtenberg, S., Horwath, M., Groh, A., Muir, A. & Gilbert, L. 2016, "A high resolution record of Greenland mass balance", Geophysical Research Letters.

Volume number and inclusive page numbers are missing.

****

McMillan, M., Shepherd, A., Gourmelen, N., Dehecq, A., Leeson, A., Ridout, A., Flament, T., Hogg, A., Gilbert, L., Benham, T., van den Broeke, M., Dowdeswell, J.A., Fettweis, X., Noël, B. & Strozzi, T. 2014a, "Rapid dynamic activation of a marine-based Arctic ice cap", Geophysical Research Letters, 2014GL062255.

Volume number and inclusive page numbers are missing.

****

Phillips, T., Rajaram, H. & Steffen, K. 2010, "Cryo-hydrologic warming: A potential mechanism for rapid thermal response of ice sheets", Geophysical Research Letters, vol. 37, no. 20.

The paper number is missing. It is L20503.

****

Scagliola, M. & Fornari, M. 2015, Main evolutions and expected quality improvements in BaselineC Level1b products.

Reference is incomplete.

****

Schenk, T., Csatho, B. & Lee, D.C. 1999, "Quality control issues of airborne laser ranging data and accuracy study in an urban area ", pp. 101.

Reference is incomplete.

****

Wilson, W.S., Abdelati, W., Alsdorf, D., Benveniste, J., Bonekamp, H., Cogley, J.G., Drinkwater, M.R., Fu, L.L., Gross, R., Haines, B.J., Harrison, D.E., Johnson, G.C., Johnson, M., LaBrecue, J., Lindstrom, E.J., Merrifield, M.A., Miller, L., Pavlis, E.C., Pietrovicz, S., Roemmich, D., Stammer, D., Thomas, R.H., Thouvenot, E. & Woodworth, P.L. 2010, "
Observing Systems Needed to Address Sea-Level Rise and Variability" in
Understanding Sea-Level Rise and Variability
, ed. Church, J.A., P.L. Woodworth, T. Aarup, and W.S. Wilson, Wiley-Blackwell, , pp. 376-399.

The publisher's city is missing.
****

I also noted that many of your references are items from the NASA National Snow and Ice Data Center Distributed Active Archive Center in Boulder. It would be nice (but not required) to give the web site.

Response:

All references have been corrected and link to NSIDC added.